U-4609

This work was performed for the Jet Propulsion Laboratory, California Institute of Technology, sponsored by the National Aeronautics and Space Administration under Contract NAS7-100.

FINAL REPORT

EFFECT OF SOLID PROPELLANT ROCKET EXHAUST IMPINGEMENT ON SPACECRAFT MATERIALS

18 March 1966 through 21 February 1969

Prepared for: Jet Propulsion Laboratory
California Institute of Technology
Pasadena, California

Under Contract: 951246

Prepared by: C. H. Lewis

19 March 1969

PHILCO Ford
PHILCO-FORD CORPORATION
Aeronutronic Division
Newport Beach, Calif. • 92663

U-4609

This work was performed for the Jet Propulsion Laboratory, California Institute of Technology, sponsored by the National Aeronautics and Space Administration under Contract NAS7-100.

FINAL REPORT

EFFECT OF SOLID PROPELLANT ROCKET EXHAUST IMPINGEMENT ON SPACECRAFT MATERIALS

18 March 1966 through 21 February 1969

Prepared for: Jet Propulsion Laboratory
California Institute of Technology
Pasadena, California

Under Contract: 951246

Prepared by: C. H. Lewis

19 March 1969

PHILCO
PHILCO-FORD CORPORATION
Aeronutronic Division
Newport Beach, Calif. • 92663

CONTENTS

ILLUSTRATIONS

ILLUSTRATIONS (Continued)

NOMENCLATURE

A	Area of incident particle stream
Cp	Specific heat of particle
c	Specific heat of target
D_p	Diameter of particle
L	Target thickness
M	Mach number
$\dot{m}_p$	Incident particle mass flux
P	Gas pressure
q	Heat transfer flux
q_o	Incident particle kinetic energy flux
R_i	Radial distance of point of interest from nozzle centerline
R_e	Nozzle exit radius
$\dot{y}$	Linear regression rate of surface
S_t	Target material shear strength
T	Temperature
T_i	Initial temperature
t	Time
u_p	Particle velocity
u_g	Gas velocity
v	Impact velocity
V	Volume of target material removed in an impact
V_o	Volume of impacting particle
Z	Distance measured from end of the normal shock region to the point of interest

NOMENCLATURE (Continued)

α	Component of impingement angle defined on page
β	Component of impingement angle defined on page
γ	Ratio of gas specific heats
δ	Cant angle of nozzle with respect to the surface
ϵ	Nozzle expansion ratio
θ	Shock angle
ξ	True impingement angle
ρ_g	Gas density
ρ_p	Impacting particle bulk density
ρ_t	Target material bulk density

SECTION 1

INTRODUCTION

This report describes the major results of work performed under JPL Contract 951246 during the period 18 March 1966 to 21 February 1969. This contract had the general objective of determining the design restraints imposed upon a spacecraft by the impingement of gases and solid particles emanating from a solid propellant rocket. The program had two phases: (1) analytic and (2) experimental. The analytic phase included a literature review of the important aspects of the problem and the development of analytic techniques to quantitatively describe the effects. This effort included a review of gaseous impingement effects, a review of hypervelocity impact work, and some developmental work on computational methods of computing gas particle flows in a high altitude rocket plume flow field.

The experimental phase was devoted to the study of the impingement damage effects on micron size particles typical of solid propellant rocket exhausts. A helium gas flow facility, a hydrogen-oxygen rocket motor and a small scale solid propellant rocket motor were used to accelerate micron size aluminum oxide particles to velocities ranging from 4000 ft/sec to over 10,000 ft/sec. These particles impinged on instrumented target samples. Effects such as material removal, particle heating, and surface alteration were studied. The existence of a particle shielding effect was determined over a range of particle flux from 8 $gm/cm^2/sec$ to 9×10^{-4} $gm/cm^2/sec$. This was found to be of prime importance in reducing particle impingement damage below that which would have been expected from single particle impaction data. Particle heating was found to be of the order of 10 percent or less of the particle incident kinetic energy flux. As a result of these experiments, further areas for future study were recommended.

SECTION 2

IMPACTION DAMAGE STUDIES

2.1 GENERAL DESCRIPTION

The objective of these studies was to gain more information about the problem of surface damage caused by multiple particle impaction of high velocity micron-sized aluminum oxide particles, such as would emanate from a solid propellant rocket motor. While considerable work has been done to date on high velocity impact of metal particles upon metal surfaces; relatively little has been concerned with multiple impactions. The experiments reported here provide a basis for delineating some of the differences between these single particle impactions and multiple impactions of micron-sized particles.

Much of the conventional hypervelocity impact data can be represented by the correlation of Sorenson[1] in which the volume of material removed per volume of impacting particle is given by

$$\frac{V}{V_o} = 0.12\left(\frac{\rho_p}{\rho_t}\right)^{1/2}\left(\frac{\rho_p v^2}{S_t}\right)^{0.845} \qquad (1)$$

If the particle impaction process could be considered as the sum of a series of independent single impactions, then the above equation could be applied directly to each impaction and the resultant material removal summed over the number of impacting particles to give the total damage. While the experiments in this study provide a test of this possibility, in reality one must consider the factors of gas-particle coupling, kinetic energy accommodation at the target surface, target surface alteration due

to material removal and/or surface hardening, and finally the effect of target ejecta on the incoming particle stream. A consideration of all these factors is necessary in the calculation of damage to a surface due to the impingement of a solid propellant rocket exhaust containing aluminum oxide particles.

2.2 EXPERIMENTAL MEASUREMENTS

The experimental program consisted of three sets of experiments. In one set helium gas was used in a Mach 5 supersonic nozzle to accelerate the aluminum oxide particles to mass average velocities between 4400 ft/sec and 5800 ft/sec. In the second set, the combustion products of a hydrogen, oxygen rocket motor were used to accelerate the particles to about 9000 ft/sec. In the third set which utilized a solid propellant rocket motor, the particle velocities were in the vicinity of 5000 to 7000 ft/sec. The aluminum oxide used in the first two sets of experiments were from a single lot and had a number peak of about 1.2 microns diameter and a mass mean of 5 microns diameter. A long slender nozzle was used to achieve maximum particle speed. One inch diameter cylindrical specimens made of aluminum alloy were used. The total surface regression of these specimens was measured and the temperature history of the specimen surface was recorded during each test. On some of the specimens surface reflectance was measured before and after the test and, on others, the micro structure of the surface was examined after the particle impactions. The third set of experiments were conducted in the high altitude rocket test facility (Cell J-4) at the Arnold Air Station in Tullahoma, Tennessee. These tests had the objective of providing information about the damage caused to actual spacecraft surface materials impacted upon by an actual solid propellant rocket motor exhaust. Some additional measurements of kinetic energy accommodation were made during these tests to provide a basis for comparison with the previously done laboratory experiments.

2.2.1 HELIUM TESTS

The helium flow facility[2] was used to produce reproducible high velocity gas particle flows into which were placed aluminum impaction samples. The facility shown in Figure 1 consists of a pebble bed heater through which the helium gas flows, a gas particle mixing system by which the particles are introduced into the heated helium stream, and a nozzle which emits into a 12-inch diameter test chamber connected to the main vacuum tank. The Mach 5 supersonic nozzle has a length-to-exit diameter ratio of 18 in order to maximize particle speed and is able to accelerate the aluminum oxide particles used in these experiments to mass average velocities between 4400 ft/sec and 5800 ft/sec. All the aluminum oxide used was from a single lot and the size distribution determined from micromeragraph runs and counting of microscope photographs indicated a number peak of 1.2 micron diameter ±0.1 micron and a mass mean of 5 micron diameter ±0.2 micron. (See Figure 2.) The pebble bed heater which was heated by hot air could

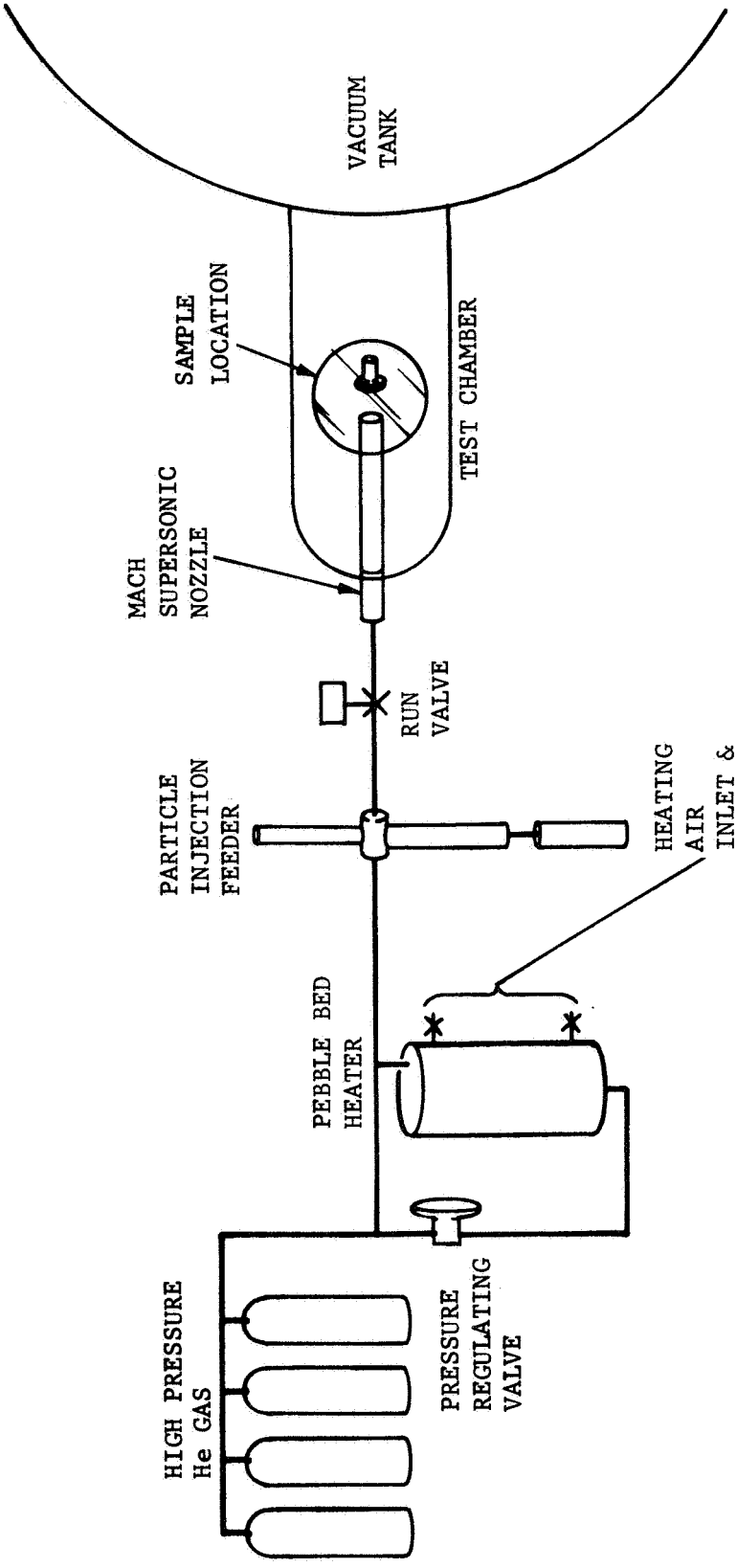

FIGURE 1. HELIUM FLOW FACILITY

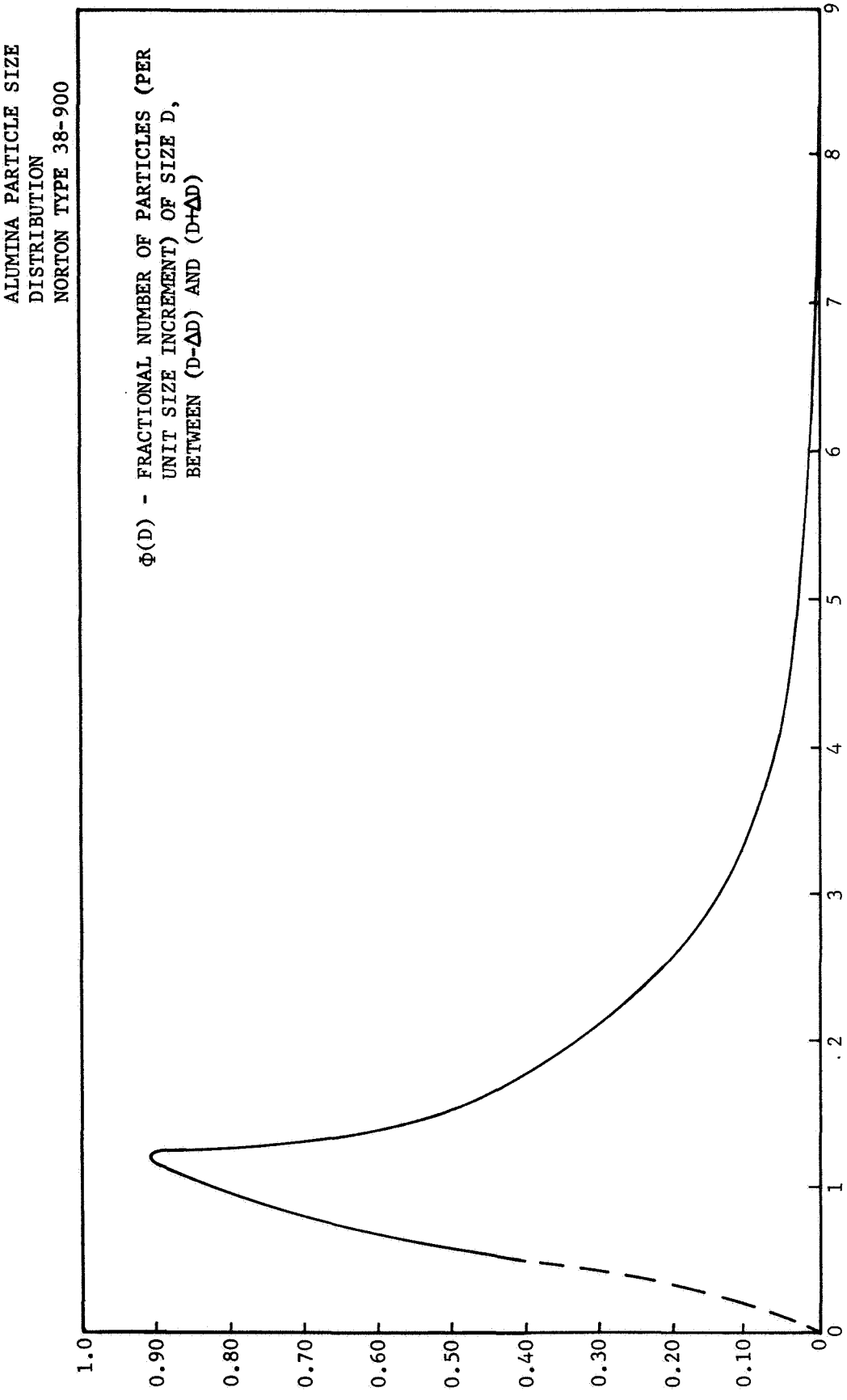

FIGURE 2. PARTICLE SIZE DISTRIBUTION

be raised to a temperature of 1000°R. This provided for helium velocities about 35 percent higher than that for room temperature helium. The helium flow lines, the particle injection feeder, and the inlet section of the supersonic nozzle were heated to the gas stagnation temperature so that during a run the stagnation temperature of the gas varied less than 2 percent of the initial stagnation temperature value. During a test, the particle feed rate is measured directly and the gas stagnation pressure and temperature are measured in order to determine the gas flow rate. Light transmission measurements are made at the nozzle exit and entrance to document the mean particulate flow velocity.[3,4] Figure 3 contains plots of the particle velocity at the exit plane of the test nozzle for different experimental conditions obtained in this study. These velocities were calculated using the Aeronutronic particle lag computer program.[5] The experimentally determined values for the particle mean velocity agree well with the theoretical calculations.

The one inch diameter, 1/8-inch thick aluminum targets used in these experiments were mounted on an insulated mounting in which were embedded heating wires so that the specimen initial temperature could be controlled. A thermocouple was mounted on the back of the test specimen in each experiment so that the initial temperature of the specimen could be determined as well as the kinetic energy input to the front surface of the specimen. In all tests, the heat loss due to gas cooling and radiation was on the order of several percent of the particle impaction heat flux. A transient heat transfer analysis indicated that the surface temperature of the specimens was within 5 percent of the measured thermocouple temperature. The samples were placed approximately 2 inches from the exit of the nozzle which is within the Mach cone of the nozzle (Figure 10b). The nozzle exit transmission measurement was made halfway between the sample front surface and the nozzle exit plane.

During initial phase of this program, experiments were conducted using 6061-T6 and 1100-0 aluminum samples over a range of particle flux from 1 $gm/cm^2/sec$ to 8 $gm/cm^2/sec$. The damage experienced by these samples using both room temperature helium and 1000°F helium was considerably smaller than that which would have been predicted by Sorenson's correlation equation.[6] (See Figure 4.) In addition, the high strength aluminum (6061-T6) was no better in resisting erosion by the aluminum oxide particles than was the essentially pure aluminum (1100-0). These results indicated the possibility of a change in the particle-surface interaction process such as a particle size scaling effect or surface work hardening, or a change in the incident particle flux properties such as would be caused by gas-particle coupling or particle-particle interaction.

In order that these results would be applicable to a spacecraft situation, the helium flow experiments had been designed so that gas-particle coupling would be small. Preliminary calculations using the two-dimensional computer program had shown that the particle velocity loss to the shock layer in front of the specimens would be small, being of the order of 2 percent for

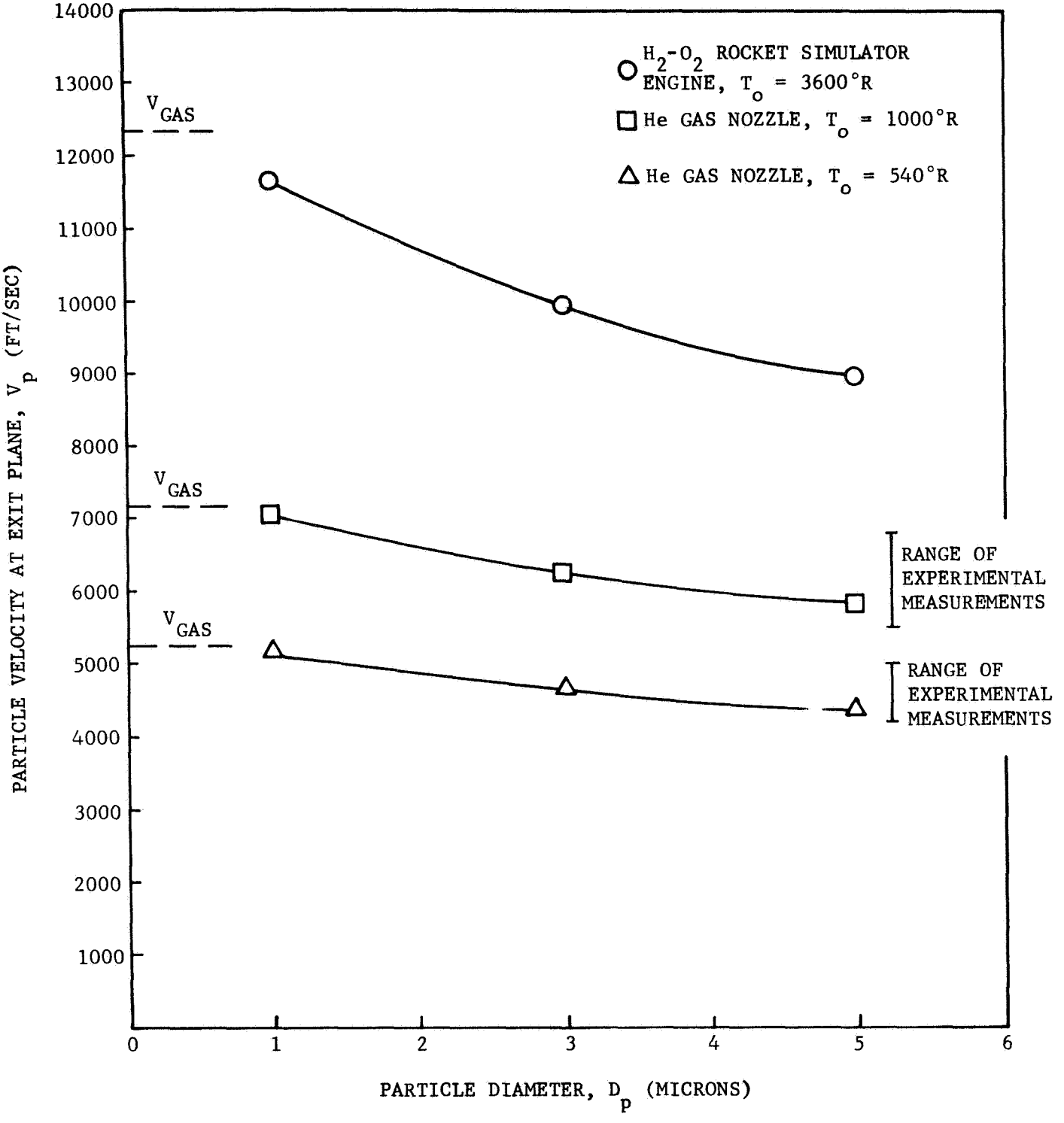

FIGURE 3. Al_2O_3 PARTICLE VELOCITY AT NOZZLE EXIT

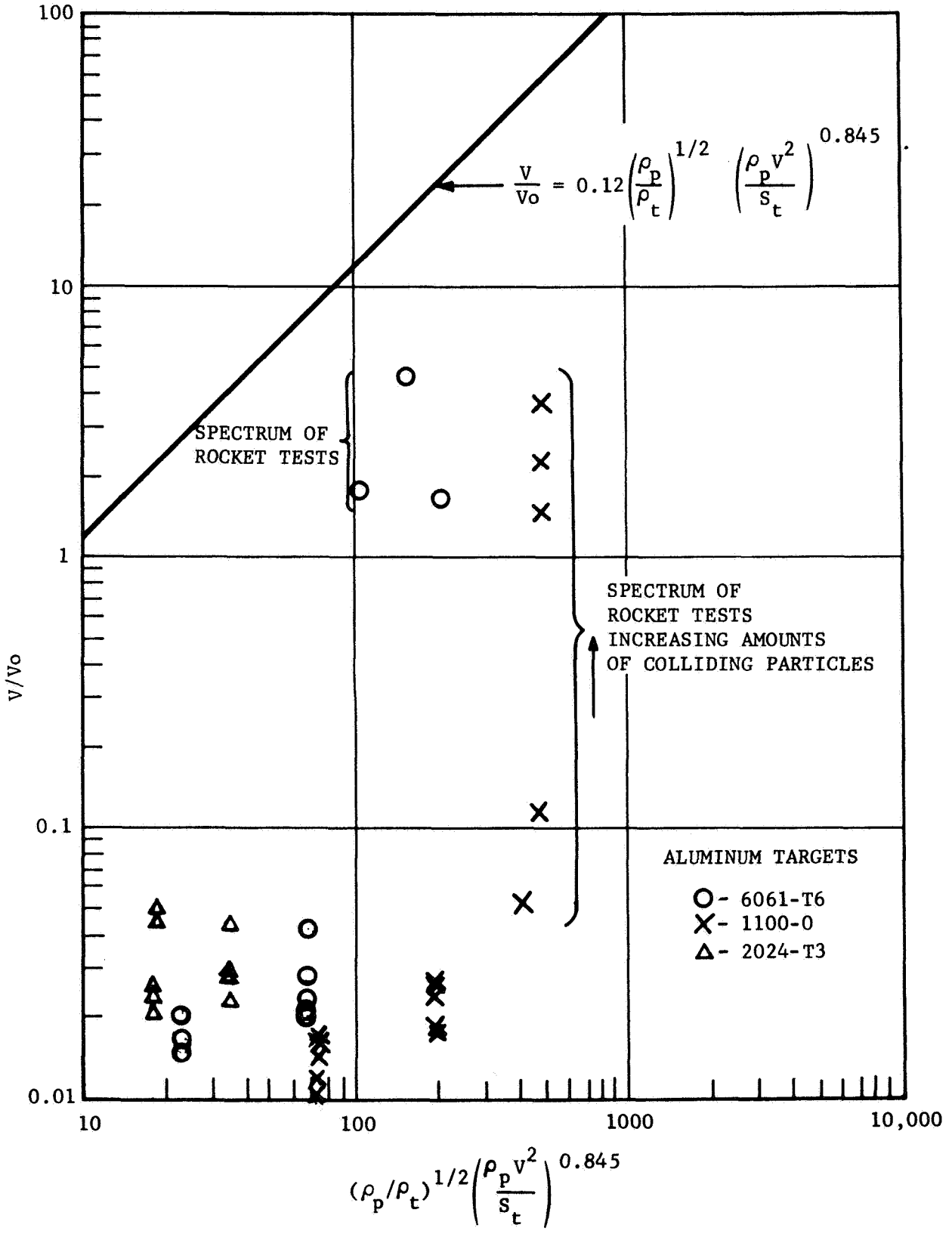

FIGURE 4. NORMALIZED VOLUME LOSS OF Al_2O_3 TO ALUMINUM IMPACTS

mean particle size and of the order of 10 percent for the number mean particle size. However, a short series of experiments were conducted to verify this in light of the greatly reduced target mass loss. Since the shock layer thickness is proportional to the specimen diameter, the specimen diameter was varied over a factor of 4, holding all other conditions constant. The variation in target mass loss, as shown in Figure 5, was relatively small and indicates that the particle velocity drop in the shock layer is also relatively small. These experiments were conducted with room temperature helium and using 1100-0 aluminum as a target material.

Additional experiments were conducted in a subsequent phase of this contract in an effort to clarify the apparent large discrepancy between single particle impaction data and the preliminary results for particle cloud impaction obtained under this contract. The helium flow apparatus provided the capability for varying particle velocity over a factor of about 35 percent, and of varying the total particle mass impacted on the specimen over a factor of 3, and for varying the particle mass flow rate of about a factor of 1-1/2, as well as varying the target specimen properties and the target initial temperature. A number of effects influencing the particle surface interaction were then studied. These effects included particle kinetic energy accommodation, the initial surface properties at room temperature, the change in surface properties at elevated temperature, and the possibility of surface hardening during the impaction process.

Particle kinetic energy accommodation was measured using aluminum specimens which were instrumented with a thermocouple mounted on the back surface. These specimens were mounted in the flow chamber on an insulated holder such that the heat loss through the rear of the specimen was small. Tests were conducted at room temperature and at 1000°R gas stagnation temperature. At the high stagnation temperature, the specimen was heated to the gas stagnation temperature by a small heating coil mounted in the holder so that the measured temperature rise would be indicative of particle impaction heating and not of gas stagnation point heating. The gas was allowed to run for a period of about a second after the conclusion of the particle impaction in order that an experimental measure of the gas cooling or heating rate could be noted. In all cases the temperature variation after the conclusion of the particle impactions was at least 50 times smaller than the temperature rise rate during the particle impactions. The three aluminum materials were tested: 1100-0, 6061-T6 and 2024-T3. The particle mass flux in all of these tests was nominally 8 grams/in.^{2}/sec, although in each test the exact flow rate was monitored and it varied somewhat about this mean. The kinetic energy accommodation factor, defined as the measured heat flux per unit area divided by the kinetic energy flux per unit area, was found to have no significant variation with either target material or particle velocity over the range tested. The value of the accommodation coefficient α ranged from a minimum of 0.05 to a maximum of 0.106 with about 75 percent of the data points falling between values of 0.075 and 0.095.

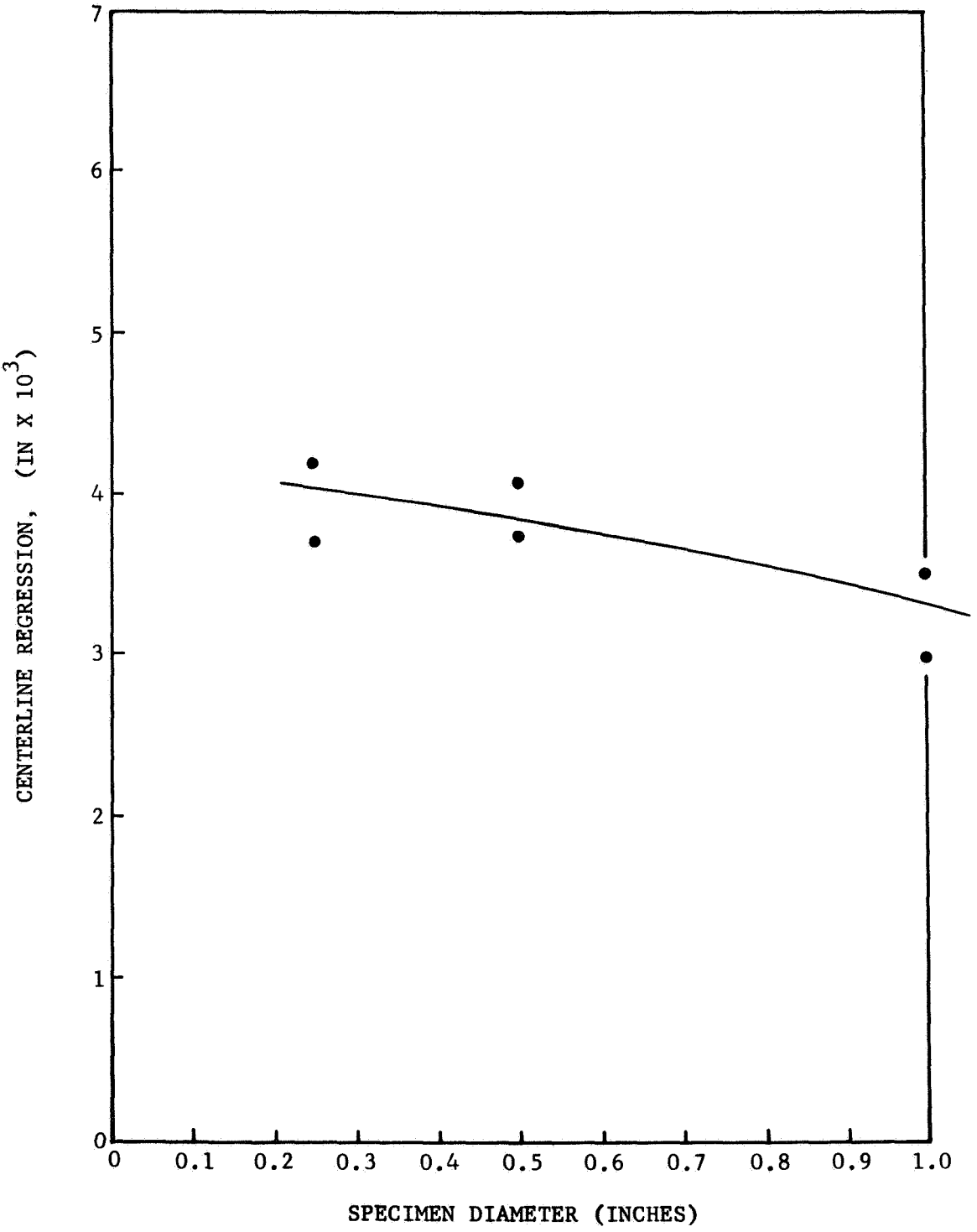

FIGURE 5. IMPINGEMENT DAMAGE AS A FUNCTION OF SPECIMEN DIAMETER

The specimens used in these tests were weighed before and after the impingement. The weight of the thermocouple was tared out as it had been weighed separately prior to being affixed to the specimens. The mass loss of the specimens determined from these weights and the measured mass flow rate of aluminum oxide particles were used to compute the volume loss ratio of Sorenson's correlation equation. The results of these tests are shown in Figure 4. Little significant difference can be seen between the two aluminum alloys 6061-T6 and 2024-T3. Both of these seem to be slightly inferior to pure aluminum 1100-0 material.

In some of the tests, the total mass particles impacted on the specimen was varied at a constant mass flow rate by varying the length of the exposure time. This time was varied by a factor of 3. These tests were conducted in an effort to detect the possibility of surface hardening. The specimens used in these tests, as well as in a number of others, were subjected to microscopic examination. Micro hardness measurements were made through the specimen interior from the front impacted surface through to the back surface which was unimpacted. No significant variation in hardness could be detected through the specimen. The hardness of the specimens varied principally with the variation of temperature history that the specimen had been through. The specimens which had been through a similar history, but which had experienced no particle impaction, had the same hardness measurements on the front surface or on the back surface as did the specimens which had been impacted by the particles.

Some measurements of surface reflectivity to visible light were made. In every case, specular reflection was reduced by about two orders of magnitude. This reduction was independent of the amount of mass loss experienced by the specimen.

2.2.2 HYDROGEN-OXYGEN ROCKET TESTS

In order to obtain particle velocities higher than those available with the helium facility, the combustion products of a hydrogen-oxygen rocket engine were used to accelerate the aluminum oxide particles through a nozzle which was similar geometrically to the one used in the helium tests.

These tests were conducted in the initial phase of this contract and, when it became apparent that it was not possible to determine the target surface temperature accurately due to the transient nature of the heating process, the tests were not continued in the subsequent phase of this program. The data obtained in these tests is of interest from a qualitative standpoint, although a quantitative determination of the surface strength during the impaction was not possible.

The aluminum oxide particles used in these tests are introduced into the combustion chamber by means of a water slurry. The chamber temperature is kept low enough so that the particles do not vaporize or melt. Thus, the

particle size distribution in a nozzle flow is known. The target location was the same as was used for the helium tests. Experimental verification of the particle velocities was not made in these tests because a light transmission apparatus was not available in the hot firing test section of the vacuum tank. Due to the geometric similarity of the two nozzles and the proven accuracy of the particle lag calculations for the helium nozzle, it was assumed with confidence that the computed values of the particle velocity were correct. (See Figure 3.)

Aluminum alloys 6061-6 and 1100-0 were used as target materials for these experiments. The test specimens were 1 inch in diameter and were about 3/8 inch thick. They were water cooled at the back surface. The aluminum temperature at the back surface was measured by a spring loaded contact thermocouple while the heat absorbed by the water was determined by measuring the water temperature inlet and outlet values and by measuring the flow rate. During the initial part of each test, the nozzle flow was free from any particles. Using the method of Fay and Riddell[7] and Boison and Curtis[8] a gas phase convective heat flux was calculated which was used in conjunction with the specimen thermocouple to determine the surface temperature prior to the impaction of any particles. Both transient calculations and examination of the specimen temperature histories indicate that the temperature distribution in this specimen reached a steady value during the gas heating period about 2 seconds in length. This equilibrium surface temperature was used in the plotting of the damage data in Figure 4. During the particle flow, additional heating occurred due to the particle impaction process. It was not possible to determine the surface temperature during particle impaction because the temperature distribution was of a transient nature during the duration of the particle impaction portion of these runs. Increasing the particle impaction duration resulted in destruction of the samples prior to the establishment of a steady state heat transfer situation. The data from these tests, shown in Figure 4, show the effect of this increased heat transfer. Proportionately more damage occurs as the amount of the impacting particles increases indicating that the surface strength is decreasing as the surface temperature is rising.

2.2.3 SOLID ROCKET ALTITUDE TESTS

The objective of these tests was to fire small 5 pound solid rocket motors at simulated altitude conditions and to determine the effects of the far field impingement of the rocket exhaust plume on instrumented target surfaces. These tests were conducted in the J4 test cell at the Arnold Engineering Development Center located at Tullahoma, Tennessee. This facility is comprised of an underground concrete chamber 100 feet in diameter and 250 feet deep, and a test capsule located on top which is 48 feet in diameter and varies in height from 8 to 81 feet. The volume of this facility is roughly 2 million cubic feet. It can be evacuated by steam ejector-blower system to a maximum pressure altitude of about 125 to 130 thousand feet.

The tests in this program were all conducted at an altitude near 130 thousand feet. The test setups were located on the flame defector platform which is situated about 50 feet from the bottom of the concrete spray chamber. (See Figure 6.) The solid propellant rocket motors used in these firings were of heavy walled construction containing about 3-1/2 pounds of polyurethane-ammonium perchlorate composite propellant. The propellant was aluminized in five of the firings at aluminum concentrations ranging from 0.08 percent up to 12 percent. One firing was made with a propellant containing no aluminum. The nozzle throat diameter used in all tests was 0.8 inch and the motors were equipped with a 40 to 1 expansion ratio 15 degrees half angle conical nozzle. The impingement targets provided by the Jet Propulsion Laboratory seen in Figures 7 and 8, consisted of a number of typical spacecraft materials. These are enumerated in Table 1.

TABLE 1

IMPINGEMENT DAMAGE TEST SAMPLES

Sample Designation	Material
2M - 6M	5 mil aluminized Mylar with aluminum facing outward.
2T - 6T	5 mil aluminized Teflon with the Teflon facing out.
2A - 6A	Polished aluminum.
2S - 6S	White paint, 5 mil thick, S13 (zinc oxide in RTV602).
2Z - 6Z	White paint, 5 mil thick, 293 (AFR-2) zinc oxide and potassium silicate.
SC3 - SC7	Solar cell
CG1 - CG4	Solar cell cover glass

Three copper slug calorimeters oriented 90-, 60-, and 20-degrees to the flow direction were used and a pitot static probe was mounted on top of a one degree of freedom force balance. A teflon disc was attached to the front surface of the force balance which was oriented 90 degrees to the flow streamlines. The damage sustained by this teflon slug in each test was used to correlate these experiments with previous laboratory experiments. Other data recorded during these tests included the rocket motor chamber pressure, the test cell static pressure and temperature, and the pressure inside the force balance body which is used in the reduction of the force balance output.

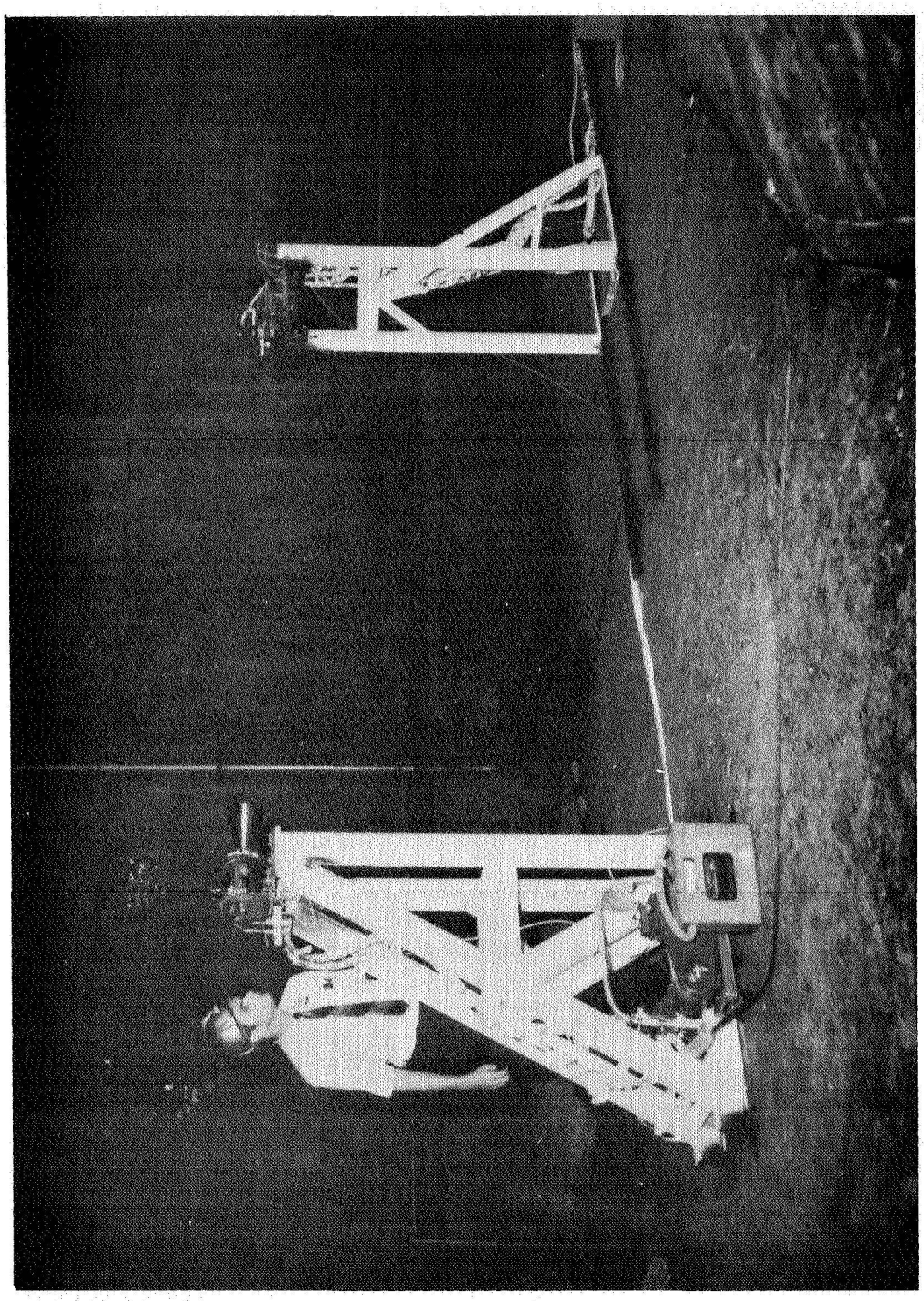

FIGURE 6. SOLID PROPELLANT ROCKET TEST SETUP

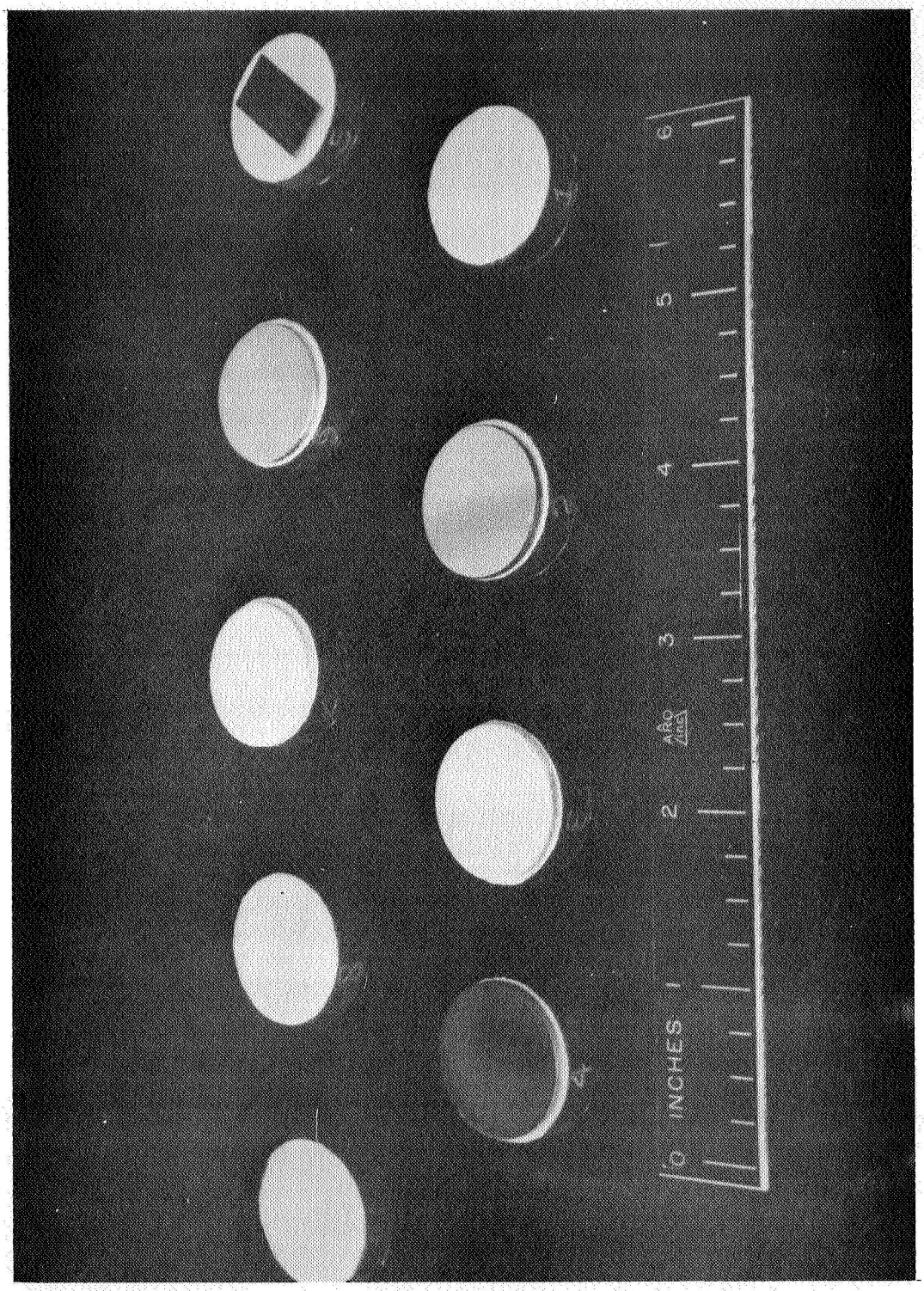

FIGURE 7. IMPINGEMENT TARGETS

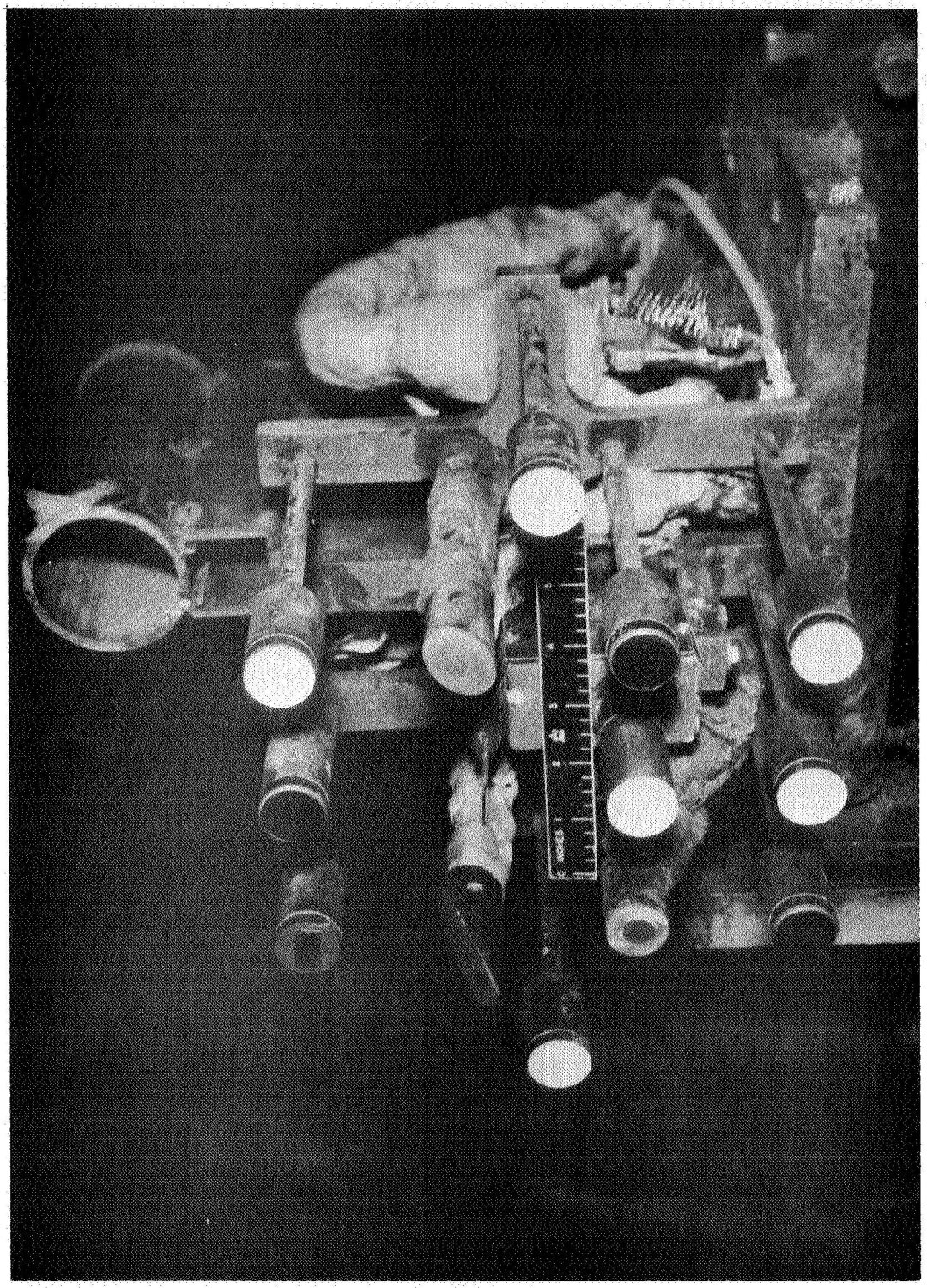

FIGURE 8. TYPICAL TARGET ARRAY

The six firings were conducted in three groups of two each. The first two firings utilized a 12 percent aluminized propellant. Run 01 was conducted with a separation distance between the nozzle exit and the target point of 100 inches, while Run 02 had a distance of 180 inches. A prediction of particle mass flux at these two stations as well as of particle and gas heating were made prior to the tests. The plume flow properties were calculated using a characteristic solution[5] and the nozzle shock was located in this flow field using the approximate method of Lewis and Carlson[9] The stagnation point heating just behind the normal shock was calculated using the method of Fay and Riddell[7] and Boison and Curtis.[8] A value of 14.9 calories per cm^2/sec was obtained. The particle flow field was calculated using the Aeronutronic particle trajectory programs. A particle kinetic energy flux was calculated at the 100-inch station of about 3.6 calories/cm^2/sec while at the 180-inch station a value of about 1 calorie/cm^2/sec was calculated. The gas heating rate, it was felt, would be equal to or less than the heating rate calculated behind the mach disc. The results of these tests, as well as those of subsequent tests, are shown in Table 2. The 90-degree heating value of 45.3 calories/cm^2/sec measured during Run 01 is considerably in excess of what might have been the estimate. The damage experienced by the target was also much more than had been expected. An examination of the mounting array for the targets showed that the particle spread was less than had been calculated, being about a factor of 2 less in radial extent at both stations. A recalculation of the particle kinetic energy flux based on a reduced radial spread gave heating values that were within 30 percent of the measured. Based on information made available by JPL, the maximum particle size in the exhaust products of this propellant operating at this chamber pressure was about 2, while the number mean was about 1 micron or less. Computer calculations of the particle projectories through the nozzle indicated that the radial spread of a 2 micron particle should have been almost to the walls of the exit cone, while, in fact, based on the results of these first two runs, the radial spread seems to be confined within a 6 degree half-angle cone. The principal uncertainty in these calculations is the particle size and velocity in the combustion chamber. The assumptions that the particles were moving with the gas velocity and were uniformly distributed across the nozzle entrance seems to have been inappropriate in this particular situation.

Calculations using the particle trajectory computer program had indicated that the particles were insignificantly affected by the gas in passing through the mach disc in these conditions. However, the uncertainty in gas heating at distances well beyond the mach disc, as well as the uncertainties in the particles flows, velocities, and directions, were great enough so that subsequent tests were conducted at an axial location which was within the mach disc. The next test, Run 03, was conducted using a propellant which contained no aluminum metal in the fuel. A measured 90-degree heating value of 14.3 calories/cm^2/sec agreed relatively well with a prediction of about 13. In this run also, the target materials were either destroyed or very seriously damaged. The gaseous heating rate measured in this run is

TABLE 2

RESULTS OF SOLID ROCKET FIRINGS

Run Number	Distance From Exit Plane	% Al in Propellant	Average Chamber Pressure	Run Time, Sec	Mass of Propellant Burnt, Pounds	Average Propellant Mass Flow, lb/sec	$\dot{Q}$-Calorimeter Heating Flux, Cal/cm^2 sec			Teflon Mass Loss Rate, $\dot{m}_t$, gm/sec	Incident Particle Mass Flux on Target* $\dot{m}_p$, gm/sec	$\dot{m}_t/\dot{m}_p$
							90°	60°	20°			
01	100 in.	12%	220 psig	4.65	3.58	0.766	45.3	25.7	5.2	0.63	0.140	4.5
02	180 in.	12	215	4.70	3.64	0.774	24.2	16.5	5.2	0.149	0.0459	3.25
03	36 in.	0	167	6.14	3.37	0.549	14.3	11.8	-	0.036	0	-
04	32 in.	0.08	168	6.10	3.43	0.562	12.8	7.6	-	0.206	0.00485	42.5
05	30 in.	0.4	160	6.19	3.74	0.604	6.9	-	1.54	0.218	0.0296	7.3
06	28 in.	2.0	171	5.80	3.78	0.645	11.2	10.7	1.95	-	-	-

*Values based on corrected particle spread determined from Runs 01 and 02 (see text).

comparable with the kinetic energy flux that would be experienced with a 12 percent Al propellant in this motor, based on the model determined from Runs 01 and 02, at a distance of about 400 inches from the nozzle exit. This indicates that at this distance the thermal effects alone would be enough to destroy these particular coatings.

All of the targets in every test were very eroded. The solar cells and the cover glasses were completely destroyed in each firing. Of the coatings, only the white paint samples had even a recognizable residue of the original coating left after any of the firings. Some of the samples were not recovered after the tests; these samples were heated to a high enough temperature to loosen the adhesive securing the sample to the holder, and the gas flow swept these targets off the deflector plate into the bottom of the test cell.

Tests 04, 05 and 06 were conducted using propellants containing 0.08 percent, 0.4 percent and 2 percent, respectively. These three tests would give an indication of the effect of a factor of 50 variation in particle flux, holding the gas heat transfer relatively constant. The remaining two sets of test materials were used with Runs 04 and 05, although it was expected that they would be virtually totally destroyed, as Run 03 had been so destructive. The principal sources of data on these runs would be the 3 calorimeters and the Teflon disc located on the front of the force balance. The pitot-static probe had been very seriously damaged during the first two runs and yielded no static pressure measurement and a very erratic stagnation pressure measurement. In Run 03, the repaired probe gave a stagnation pressure value which agreed with prediction; however, the static pressure probe gave a suspiciously high reading and continued to do so through the remainder of the firings, so that a leak in the line somewhere has been suspected. The heat flux measurements for Runs 03 through 06 were all relatively consistent with each other. Some difficulty was experienced with Run 05 such that the 60 degree measurement was not obtained and the 90 degrees seems to be in question, due to high resistance connections in the cell. The Teflon damage obtained on Runs 03, 04 and 05 was of particular interest. The specimen had been inadvertently omitted on Run 06 so this data point was lost. Run 04 clearly indicates the effect of the particle impaction process from the standpoint of mechanical erosion. The heat flux to the Teflon disc was essentially the same in Run 04 as it was in 03 except that the damage is almost 6 times greater. The amount of Teflon material removed on a weight basis was over a hundred times greater than the mass of impacting particles. Run 05 indicates the possible existence of a phenomena which has been under study in a concurrent program conducted at Aeronutronic, in that an increase in particle flux of about a factor of 5 increases the damage very slightly and produces a mass removal ratio of about 30, which is about a factor of 4 less than Run 04.

2.3 DISCUSSION OF EXPERIMENTAL RESULTS

During the course of this contract, another experimental program was initiated at Aeronutronic which had the purpose of determining the forces generated on surfaces which had been impacted upon by solid propellant exhaust plumes.* During initial measurements of forces in this program, it became apparent that the force which was being measured on 90 degrees inclined surfaces in the flow was essentially that of an inelastic force.[10] When this was compared with the measurement of kinetic energy accommodation on a similarly oriented target made under this contract, which seemed to indicate a relatively elastic collision, in that the accommodation coefficient is of the order of 0.1 or less, the existence of the possibility of target shielding became more apparent. As the SAMSO program was concerned with the force generation on ablative material surfaces, as a matter of course from the tests in this program, damage data became available. One of the materials used in the program was Teflon. The damage data for the Teflon tests indicated that the damage experienced by the Teflon was extremely nonlinear with incident mass flux. The mass of target material removed per mass of incident particles decreased markedly as the incident particle mass flux was increased.[10] This brought to light that, in addition to a possible size scaling[11,12] effect, there was definitely an alteration of the particle stream by an interaction with the environment immediately surrounding the target.

As previously noted, the two most obvious interaction mechanisms are gas-particle coupling and target shielding. In the former case, particles are deflected from the incident stream by virtue of the drag exerted by the gas flowing around the target, while in the latter case, incident particles are removed by collisions with impact debris ahead of the target. Both processes would reduce the target damage below the undisturbed value as well as decreasing the kinetic energy flux to the surface and could, in addition, reduce the impact force on the surface. However, for the flow conditions used on the force measurement tests, as well as for the conditions in this work, gas-particle coupling is sufficiently small to be within the uncertainty of the incident particle velocity, so one is drawn to the conclusion that the principal effect of these two must be target shielding. The qualitative observation that initially flat targets tend to become rounded with minimum surface regression at the center upon being impacted by a particle cloud, also supports an interaction mechanism.

For instance, the debris in the shielding layer would be relatively at rest near the center of the target where the gas motion is slow, while near the edges the debris would be swept along with the expanding gases. Thus, the debris layer would be more effective in shielding the target at the center than at the edges. For oblique impact, particles entering the shock layer at increasing distances from the target tip would require less deflection to avoid impinging on the rear of the target, so that in agreement with

*This program was funded under SAMSO Contract No. FO 4694-67-C-0051.

the experimental observations of the SAMSO program,[10] less surface regression would be experienced there. Likewise, since the mean motion of both debris and gas flow is toward the rear of the target, the debris layer should thicken and provide greater protection to the target with increasing distance from the tip. As a comparison between the SAMSO results and the results of this program was useful in establishing the existence of a debris layer, a further comparison will be used on specifying the source of the debris. For the aluminum targets used in this program the maximum ratio of mass of target removed to total mass of impinging particles was very small compared to unity. In the SAMSO work, this ratio for metals was also very small compared to unity, while for the ablating materials tested, the factor was of the order of unity or less. Thus, the mass addition from the target increased the total concentration of particulate matter around the target by at most a factor of 2 for ablating materials and negligible for metals. Also, the force measurements for the stainless steel targets in the SAMSO work which experienced negligible mass loss exhibited the same behavior as the ablative materials. It seems reasonable, therefore, that the steel targets would also be subjected to the same shielding effects as observed for the ablators. Both of these factors indicated that in these tests the impact debris is comprised primarily of spent particle material. The size of debris in this layer remains uncertain. Since aluminum is a brittle material, it is probable that the particles fragment on impact, so that on the average the debris is smaller than the incident particle projectiles. Teflon damage data obtained from experiments in this contract, as well as the SAMSO contract are plotted on Figure 9. It can be seen that target mass loss ratios over a 100 were obtained in the solid rocket firings at Tullahoma. In these tests, the target experienced a very high mass loss compared to the incident particle flux; however, it is uncertain as to what form the target material was in as it was removed. It is possible that it was in the form of gas evolution at the surface, or a liquid layer which washed around the target and carried away at the corners by the gas stream flowing by, or possibly fragments of Teflon which were released by the force of the incoming particle impactions. In any event, a comparison amongst these tests and a comparison of these tests with the experimental tests done in the helium flow facilities indicates that the process of shielding in all of these tests seems to be similar.

An interesting visualization of the particle shielding layer can be seen in Figures 10a and 10b. These photographs were obtained in the helium test facility used in this contract and utilized the photographing of 90 degrees scattered light from the particle cloud around the target. The targets were illuminated from above, using a General Electric BH-6 Mercury Arc Lamp which was collimated to produce a narrow sheet of light parallel to the flow axis. Similar photographs were obtained using a transmission method and a simultaneous schlieren observation in the SAMSO work.[10] The nozzle exit plane is on the right hand side, and the incident particle stream is well defined against a dark background by a low intensity of scattered light. The debris layer immediately adjacent to the exposed surface of the target is clearly obvious, and the brightness of this zone contrasted

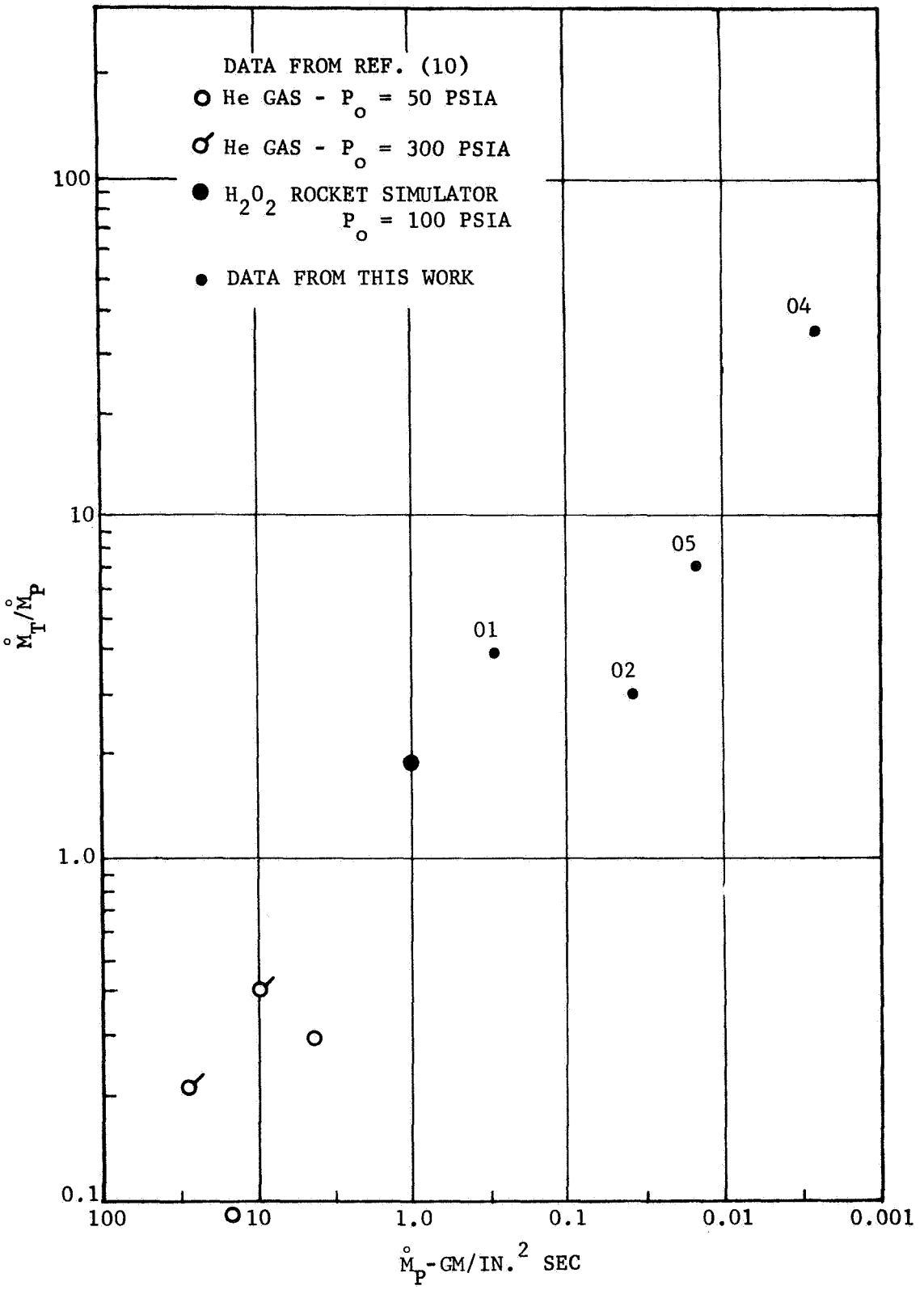

FIGURE 9. NORMALIZED TARGET DAMAGE AS A FUNCTION OF PARTICLE MASS FLUX

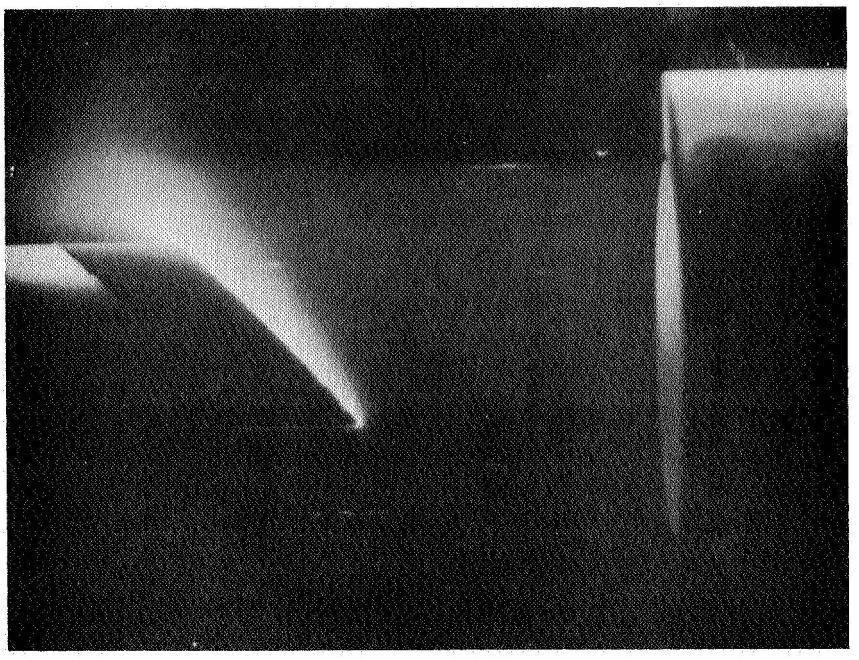

CCP TARGET, 45°

TFE TARGET, 45°

FIGURE 10a. 45° LIGHT SCATTERING RECORDS OF DEBRIS LAYER. FLOW FROM RIGHT TO LEFT

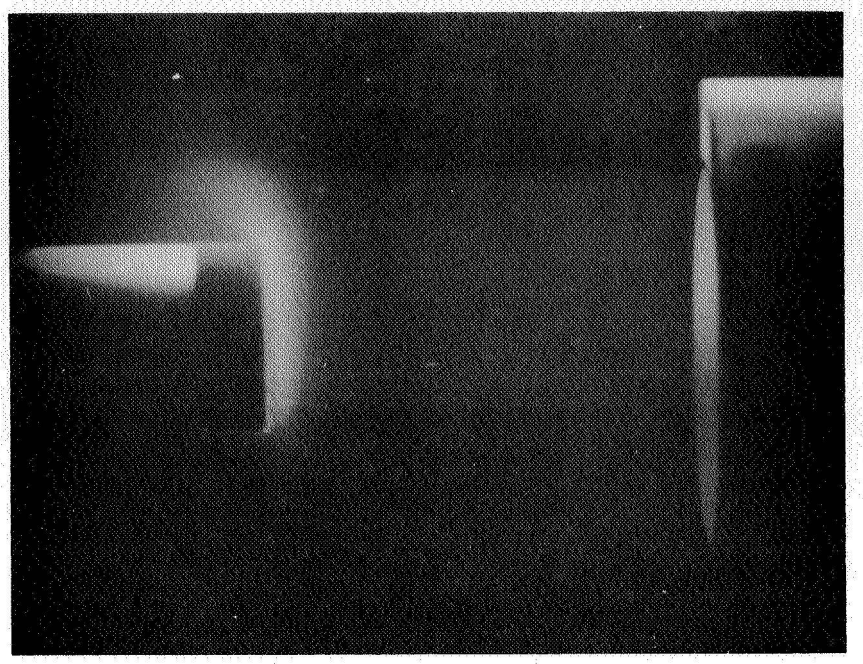

CCP TARGET, 90°

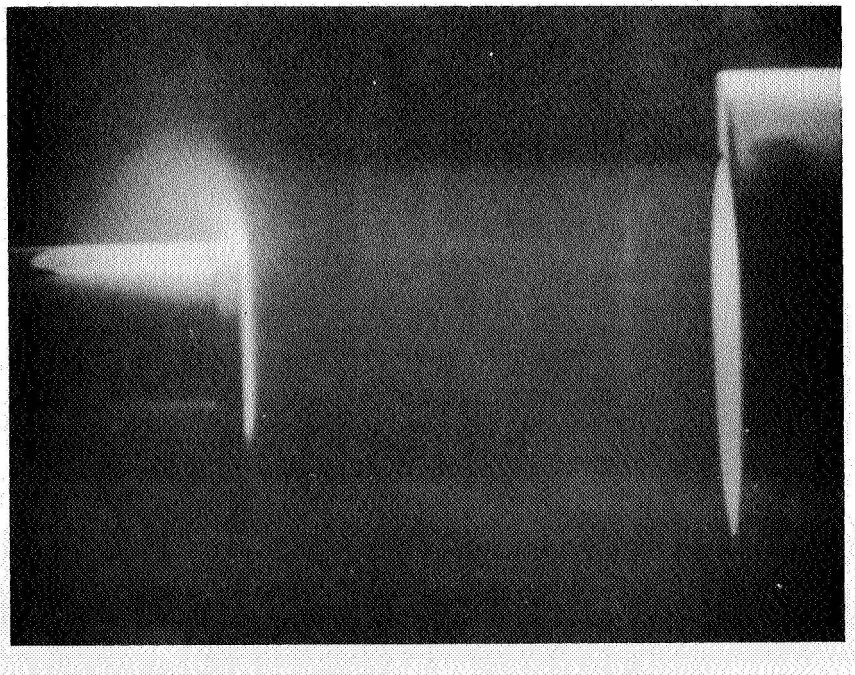

TFE TARGET, 90°

FIGURE 10b. 90° LIGHT SCATTERING RECORDS OF DEBRIS LAYER. FLOW FROM RIGHT TO LEFT

to that of the incident stream is a qualitative measure of the density of the layer. Carbon cloth phenolic targets were utilized, as well as Teflon and aluminum. The CCP material was included, as it was another typical ablative material, yet one which was easily damaged, and one that had decidedly different properties compared to Teflon. The layer ahead of the CCP targets in Figures 10a and 10b appears to be thicker, and the leading edge more diffused than that of Teflon. Aluminum targets looked very similar to Teflon. This difference may be due to the possibility that the material removed from the CCP targets might be particulate matter with enough velocity to diffuse further away from the surface, while the material evolved from the Teflon surface may be mainly gaseous; however, there are some considerations which may negate much or all of this apparent difference. First, light from the incident beam which reflects from the surface of the target can also scatter in the direction of observation in an amount dependent on the reflectivity of the surface. Second, the CCP contains carbon which is an efficient emitter, and if present in the debris layer, may also contribute to the apparent aluminosity of the layer. The edge of the CCP target was observed to glow red hot during the tests and this, in fact, accounts for the thin bright line delineating the surface of the target in Figure 10. Third, the debris layer itself is heated to elevated temperatures during the impingement process, and the self-aluminosity of the layer was sufficiently intense compared to the scattered light intensity to be recorded on photographs taken without the light source.

At this point, it becomes clear that not only does a target shielding effect exist, but that there exists a range of conditions of interest where this effect is a very significant, if not the dominant effect, controlling the particle impaction process. It is of interest to note that the influence of shielding is considerably different when one considers the accommodation of either particle momentum or the accommodation of particle kinetic energy and particle induced damage. The particle impingement force has been seen to be influenced by the variation of particle incident mass flux to a relatively small degree;[10] however, the particle induced damage and kinetic energy accommodation are strongly dependent on the particle incident mass flux. For instance, note the results of Figure 9. As a result of interparticle collisions within the debris layer, only a small fraction of the incident energy reaches the target surface, while a major fraction of the incident particle momentum diffuses through the layer to the surface.

At sufficiently low particle mass flux, the incident particles reached the target without interference. As the particle mass flux increases, the layer becomes thick enough so that collisions between incident and reflected particles become more frequent. As a result, some of the reflected particles are scattered back toward the target and strike a second time. Eventually, at high enough particle mass fluxes, none of the incident particles strike the target surface without having experienced at least one collision in the particle layer. In other words, the particle-particle mean free path has become on the order of the thickness of the layer or smaller. Consequently,

an individual particle experiences many collisions and may, in fact, impinge on the surface a number of times before either being scattered or convected from the layer. The result of this process is a considerable reduction of the average velocity of particles striking the surface. Since the momentum of the particle stream is conserved, the reduced velocity must be compensated for by an increase in the number of impinging particles. Thus, the impact force is essentially unaltered by the presence of the debris layer except for those particles which are either scattered out of the layer or are convected about the surface by the gas stream. As impact damage is known to be highly velocity dependent, as shown in Equation (1), a significant decrease in the approach velocity will be accompanied by a reduction in the target mass loss.

The results shown in Figure 9 are an indication of this process; in that as the particle mass flux was reduced, the damage caused per impacting particle was continuously increased. If one had usable single impact data for, in this case Teflon, he would expect that ultimately the data, such as shown in Figure 9, would approach the value for a single particle impact. It is of interest to note that the data from the solid propellant rocket firings was damage data for a surface that was at or near the sublimation temperature of Teflon (800°C). Thus, in attempting to apply these data to a situation, where the gas heat transfer was greatly reduced or for all practical purposes nonexistent, a considerable over-statement of the damage would be obtained.

If, as noted above, the energy flux incident on the target is reduced by the interparticle collisions within the debris layer, then it follows that the debris layer must act as a sink which absorbs the kinetic energy of the free stream particles. In addition, since the debris material moves with a relatively small velocity, it follows that the thermal energy of the layer must be very great compared to its kinetic energy. Thus, it is of interest to consider the consequences of a simple model of one-dimensional heat transfer to the surface. The target used in the thermal-accommodation measurements was an aluminum disc, 0.32 centimeter thick, attached to an insulating backing material and subjected to particle impingement on the front surface. The temperature drop across the target was small compared to its mean temperature, while the heat conducted across its rear surface was negligible compared to the energy absorbed by the target. The appropriate energy balance for this case can be written as

$$\frac{d}{dt}\left[\rho_t LC\left(T-T_i\right)\right] = q_o - \dot{m}_p C_p \left(T-T_{ip}\right)/A \qquad (2)$$

where L is the instantaneous target thickness and it has been assumed that the target surface and debris material are in thermal equilibrium. Expanding Equation (2), and substituting $dL/dt = \dot{r}$ and $L - L_o = \dot{r}t$, where L_o is the initial target thickness yields

$$C\rho_t\left(L_o - \dot{r}t\right) d\left(T-T_i\right)/dt = q'_o - \dot{r}\rho_t C\Gamma\left(T-T_i\right) \qquad (3)$$

where

$$q'_o = q_o + \left(\dot{m}_p C_p / A \right) \left(T_{ip} - T_i \right)$$

and

$$\Gamma = 1 + \dot{m}_p C_p / \dot{r} \rho C A$$

This can be integrated to obtain the temperature time history of the target:

$$T - T_i = \frac{q'_o}{\dot{r} \rho_t C \Gamma} \left[1 - \left(1 - \frac{\dot{r} t}{L_o} \right)^{\Gamma} \right] \tag{4}$$

Finally, taking the time derivative of the Equation (4), one obtains

$$\frac{dT}{dt} = \frac{q'_o}{\rho_t C L_o} \left(1 - \frac{\dot{y} t}{L_o} \right)^{\Gamma - 1} \tag{5}$$

substituting typical test values into Equation (5) ($q'_o \sim = 560$ cal/cm^{2}sec, $\Gamma = 14, \dot{r} = 0.04$ cm/sec, $L_o = 0.32$ cm yields, at time t = 1 sec, dT/dt = 580°C/sec. This figure is several times greater than the 160°C/sec measured experimentally. This, then, is a direct indication that the target temperature is less than that predicted by the analysis, and that therefore, that the temperature of the debris layer must be greater than that of the target. This conclusion has some verification in fact, as considerable radiation can be seen from the debris layer in front of aluminum targets using the helium facility. The emissivity of aluminum oxide increases drastically upon melting so that, to produce appreciable radiation, it is quite probable that the aluminum oxide would have to have reached melting temperature (over 3000°F).

The above analysis indicates one further point that is of interest. Very small particle fluxes, if experienced over along period of time, even in the absence of gas heating, could cause a sufficient temperature rise such that the particle induced damage could be considerably greater than that calculated for a cold surface. The physical properties of aluminum alloys as well as Teflon and probably a number of paint materials are all sufficiently temperature sensitive so that not only the initial temperature of the surface should be known, but also the variation of the temperature of the surface during the particle impactions. In order to be able to do this, it is obvious that more experimental measurements would have to be made of typical surface materials over a range of temperatures that might be possible and at particle mass fluxes that would be typical of cases of interest.

SECTION 3

GASEOUS PLUME IMPINGEMENT EFFECTS

In the initial phase of this program, a survey of the methods of evaluating the effects of gaseous rocket exhaust plume impingement was made. The emphasis was on the development of a hand-book type procedure for making engineering estimates of the pressure and heat transfer on a surface located within an exhaust plume. The following discussion will be limited to highly underexpanded plumes. Regions in which a plume shock could impinge on the surface are excluded because the resulting flow field would be beyond a handbook approach.

Any calculation of plume impingement effects is dependent upon the determination of reasonable exhaust plume profiles. These profiles should define the following local properties within the plume: (1) flow direction, (2) flow velocity, (3) statis temperature, (4) static pressure, (5) local gas specific heat, and (6) gas molecular weight. The exhaust plume computer program[5] can be used to determine all of these parameters at any location within the plume. The effects of the gas plume impingement in two phase flow impingement situations become small with respect to the solid particle effects as the distance from the nozzle is increased. Therefore, no attempt will be made to describe the impingement effects of the gaseous plume in the rarefied or noncontinuum flow regime. For most practical applications, flow with a freestream Mach number at 12 or greater is outside the continuum regime. The plume computer program utilizes the method of characteristics, which reguires the assumption of flow continuity. Although this program is capable of developing the exhaust plumes beyond flow Mach numbers of 12, its use in these regions is highly speculative. Calculations of the gas plume impingement pressure and heating may be made, at large Mach numbers, but the accuracy diminishes rapidly. In most cases the computed heat transfer and pressure are conservatively high.

3.1 PLUME IMPINGEMENT (UPSTREAM PROPERTIES AND TRUE ANGLE)

Schlieren photographs of highly underexpanded plumes impinging on large flat surfaces indicate that the impingement shock waves tend to remain close to the surface (see References 13 and 14) when the nozzle exit plane is more than one nozzle diameter from the surface and parallel to or canted outward from the surface. Under these conditions the impinging flow Mach number is generally greater than 5 and the conditions of hypersonic flow are applicable. To simplify the calculation of the flow properties at the surface, it will be assumed that the shock layer is very thin and lies very close to the surface. It is further assumed that (1) the boundary layer growth and mass addition do not lift the shock layer off the surface and (2) reflected shocks emanating from the nozzle do not affect the plume flow. Thus, it is possible to obtain the gas properties impinging on the surface by direct superposition of the surface in question on the fully developed plume profile. Essentially, this means that the plume flow field is not turned, distorted, or otherwise affected by the object being impinged upon until the plume actually impacts the surface of the object. Thus, with a scale drawing, the undistorted plume properties and true impingement angle (the smallest angle between the streamline and a plane tangent to the surface at the point of impingement) can be found at the point of concern on the intersecting surface or object. By turning the flow through the true impingement angle, the local surface static pressure, temperature, and Mach number can be computed.

Figure 11 illustrates the superposition of an exhaust plume profile on a flat surface. From this figure it is obvious that the centerline impinging flow properties and true impingement angle can be directly determined, and in many cases a calculation of the surface pressure and heating on the centerline is sufficient for engineering estimates of the magnitude of the problem. However, in actual design applications it is often necessary to estimate the off-centerline pressure or heating profile which involves more complex trigonometric considerations. The following few paragraphs are devoted to illustrating the solution of the true impingement angle for several plume-surface impingement situations commonly encountered in spacecraft application.

The exhaust plume must first be defined graphically such that the angle between the nozzle axis and the line tangent to the streamline at the point of impingement can be determined (see Figure 11). Figures 11 and 12 illustrate a common situation where a nozzle is fired above a flat surface which is parallel to the nozzle axis ($\delta = 0$) and displaced radially from the nozzle a distance (r). The true impingement angle (ξ) for any point on the flat surface can be computed using the following equations:

$$\xi = \sin^{-1} (\sin \alpha \sin \beta)$$

UNCANTED NOZZLE FIRING OVER A FLAT SURFACE

— — — Lines of Constant Local Flow Properties P,M,T,γ

——— Flow Streamlines

▬▬ Location of Centerline Impingement

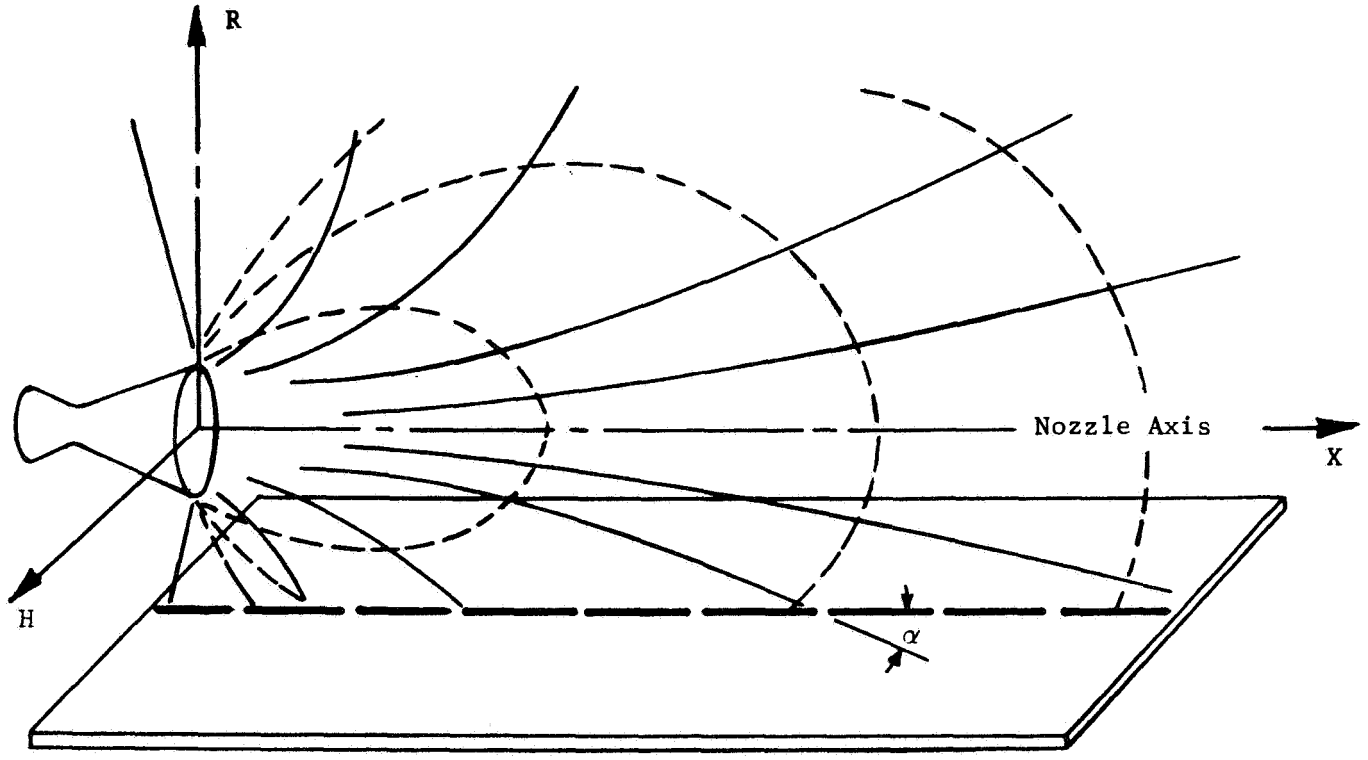

- α = True Impingement Angle for Centerline Case
- Impingement Surface Drawn Parallel to Nozzle Axis but Perpendicular to the Plane of the Plume (R-X)
- The Line on the Surface Called the Centerline is Defined by the Locus of Points Contained by Both the Plane of the Plume (which also Contains the Nozzle Axis) and a Plane which is Tangent to the Surface and Perpendicular to the Plane of the Plume

FIGURE 11 - ROCKET PLUME IMPINGEMENT ON A FLAT SURFACE (CENTERLINE CASE)

TRUE IMPINGEMENT ANGLE FOR UNCANTED NOZZLE
FIRING OVER A FLAT PLATE

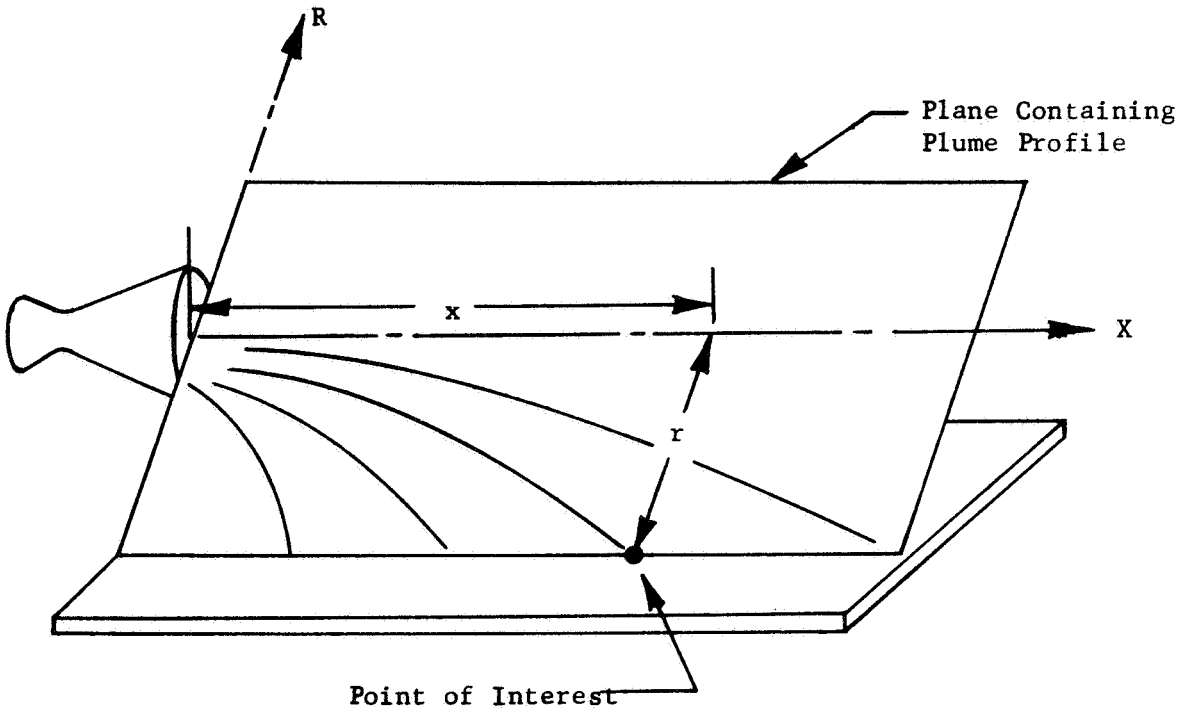

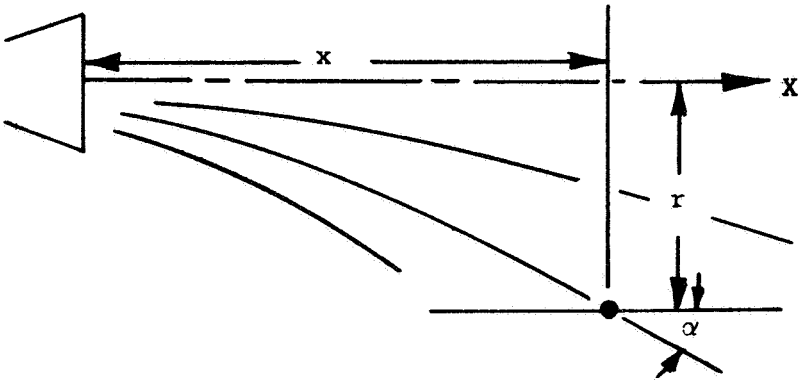

Plane View of Plume Profile

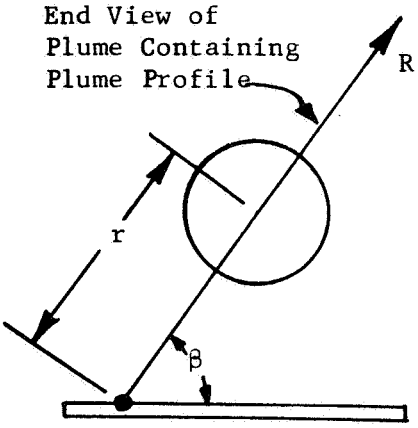

End View of Nozzle

FIGURE 12- ROCKET PLUME IMPINGEMENT ON A
FLAT SURFACE (OFF CENTER CASE)

where:

$\alpha \equiv$ angle between the nozzle axis and the tangent to the streamline at the impingement point.

$\beta \equiv$ angle between the projected plane containing the streamline and the line tangent to the surface at the point of impingement in a plane parallel to the R-H plane.

Figure 13 illustrates the more general situation of a canted nozzle ($\delta \neq 0$) firing over a flat plate.

$$\xi = \sin^{-1} (\cos \delta \sin \alpha \sin \beta - \sin \delta \cos \alpha)$$

where:

$\delta \equiv$ cant angle of nozzle with respect to the surface.

One of the more difficult solutions is that for a situation similar to a roll moment producing rocket firing over the surface of a cylindrical spacecraft. Figure 14 illustrates the geometric variables required to determine the true streamline impingement angle. The solution of the true impingement angle (ξ) can be found by using the variables illustrated in Figure 14 in the following equations:

$$\mu_o = \sin^{-1} \frac{x + h}{a_o}$$

$$\theta_i = \sin^{-1} (R_q/R_i)$$

$$\xi = \sin^{-1} (\cos \mu_o \sin \alpha_o \sin \theta_i - \sin \mu_o \cos \alpha_o)$$

Probably the most common use of solid propellant motors on space booster systems has been posigrade and/or retrograde stage separation. In this application the motor fires axially over the cylindrical surface of the booster or spacecraft (see Figure 15). The solution of the true impingement angle is, of course, easier for the off-centerline cases if the axis of the nozzle is parallel to the axis of the cylinder. However, nozzles canted outward from the surface are more common. Solutions for both cases are presented below.

Zero degree cant angle ($\delta = 0$):

True impingement angle $\xi = \sin^{-1} (\sin \alpha_i \sin \beta_i)$

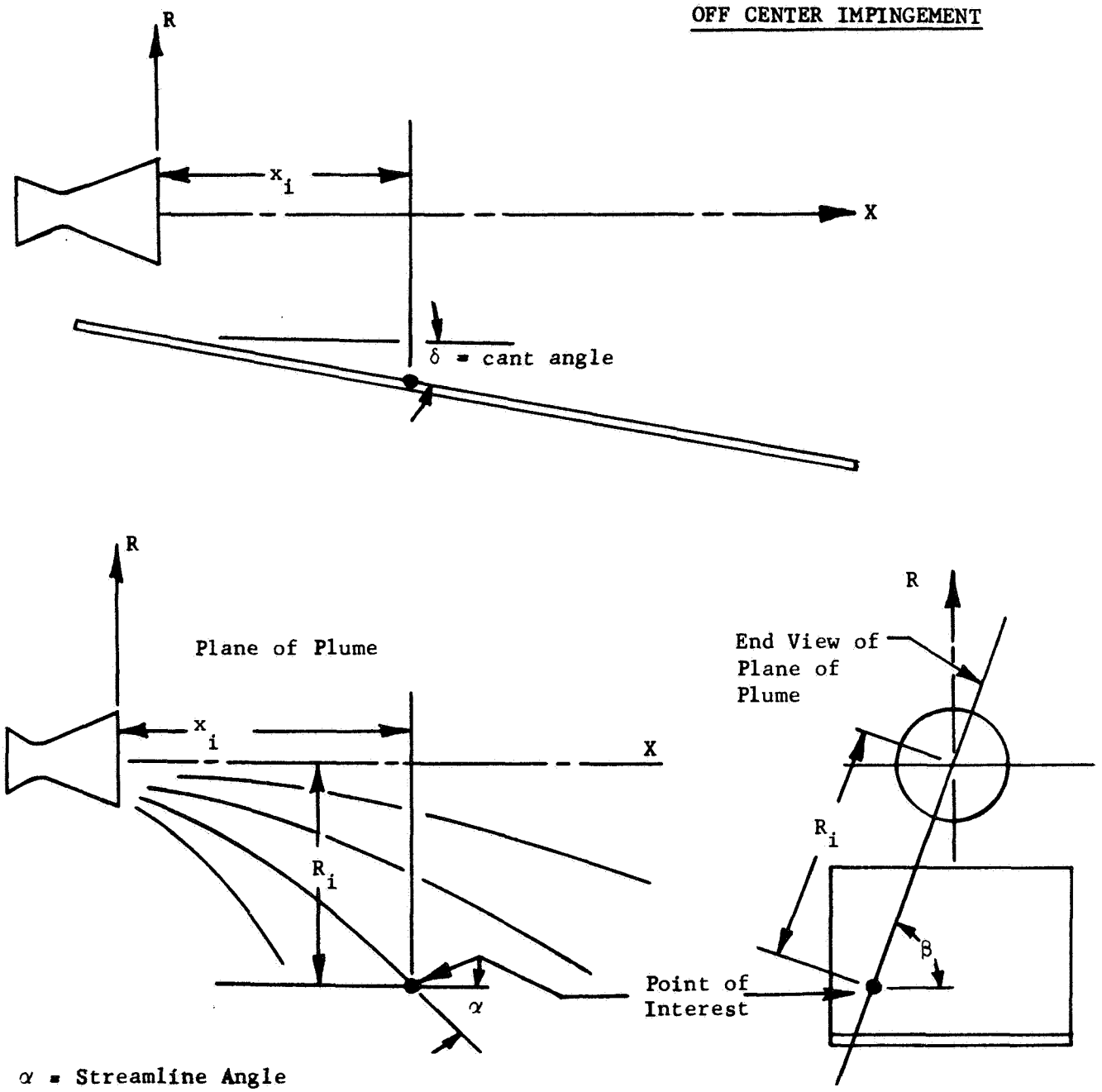

FIGURE 13 - ROCKET PLUME IMPINGEMENT
ON A FLAT SURFACE

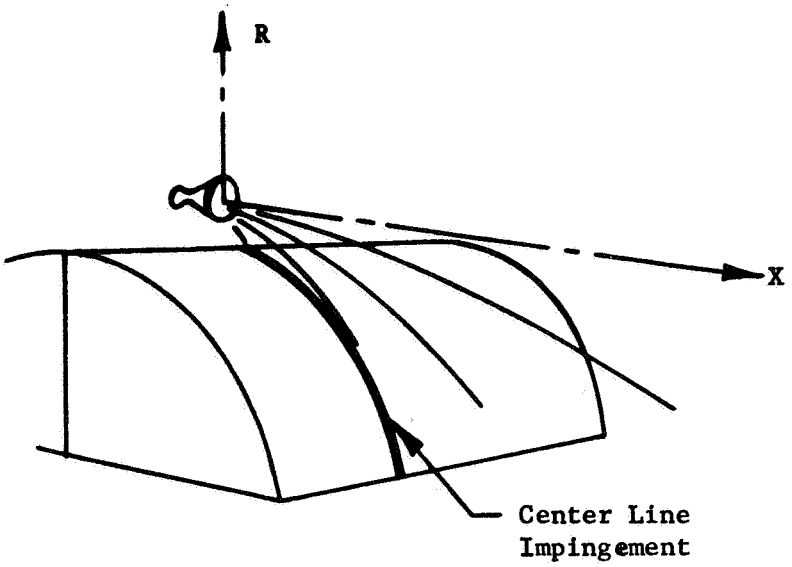

CENTER LINE IMPINGEMENT

- Plume Shown in R-X Plane
- R-X Plane Perpendicular to Cylinder Axis
- Impingement Properties and True Impingement Angle Read Directly

---

OFF CENTER IMPINGEMENT

- All Dimensions Normalized on the Nozzle Exit Radius
- α_o - Angle Between the Streamline and the Nozzle Axis at the Point of Interest

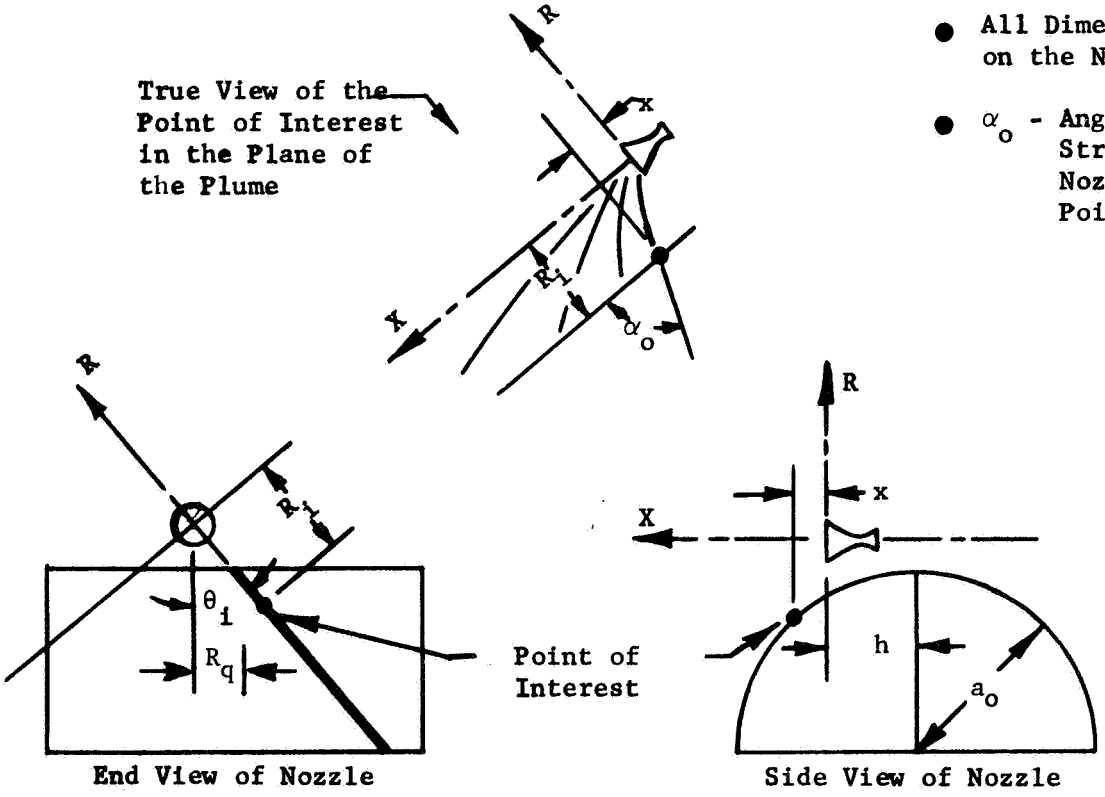

FIGURE 14. **ROLL ROCKET PLUME IMPINGEMENT ON A CYLINDRICAL SURFACE**

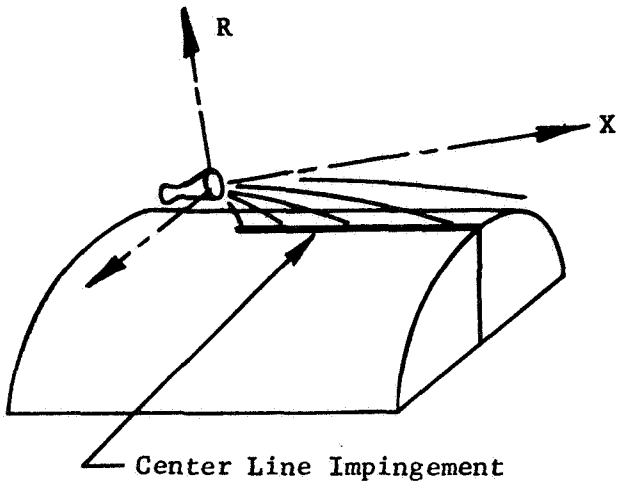

CENTER LINE IMPINGEMENT

- Plane of Plume Contains Axis of Cylinder
- Nozzle Axis (X) may be Parallel to or Canted to Cylinder Axis ($\delta \geq 0$)
- Impingement Properties and True Impingement Angle Read Directly

---

OFF CENTER IMPINGMENT
Uncanted Nozzle ($\delta = 0$)

- α_o = Angle Measured Between the Nozzle Axis and Streamline at the Point of Interest
- All Dimensions Normalized By Nozzle Exit Radius

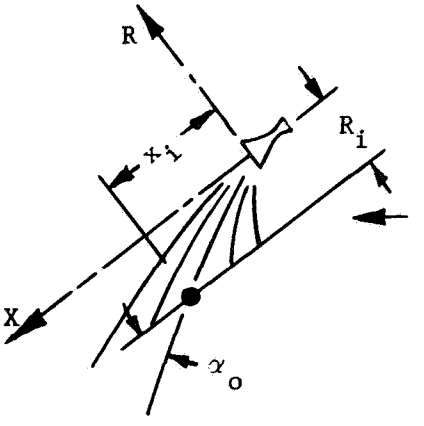

True View of the Plane Containing the Plume, Nozzle Axis, and the Point of Interest On the Cylindrical Surface

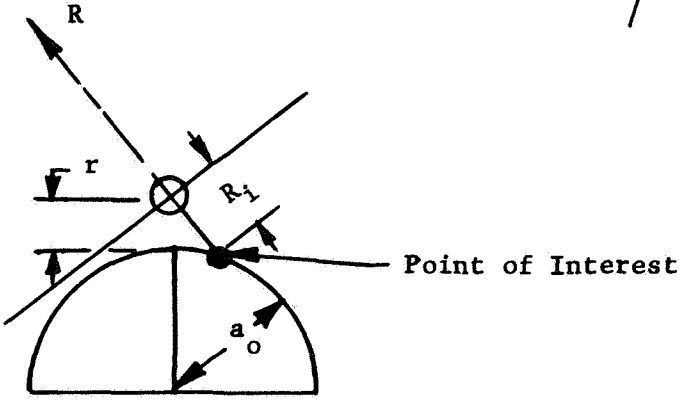

End View of Nozzle

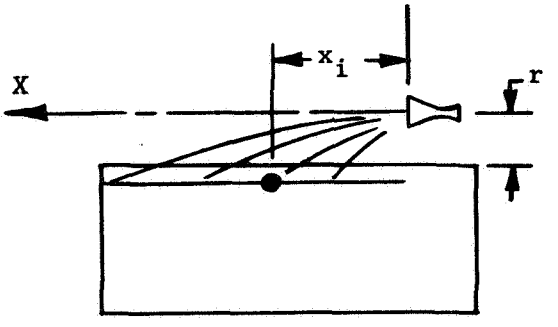

Side View of Nozzle

FIGURE 15a. **PITCH OR YAW ROCKET PLUME IMPINGEMENT ON A CYLINDRICAL SURFACE**

Off Center Impingement

(Canted Nozzle $\delta > 0$)

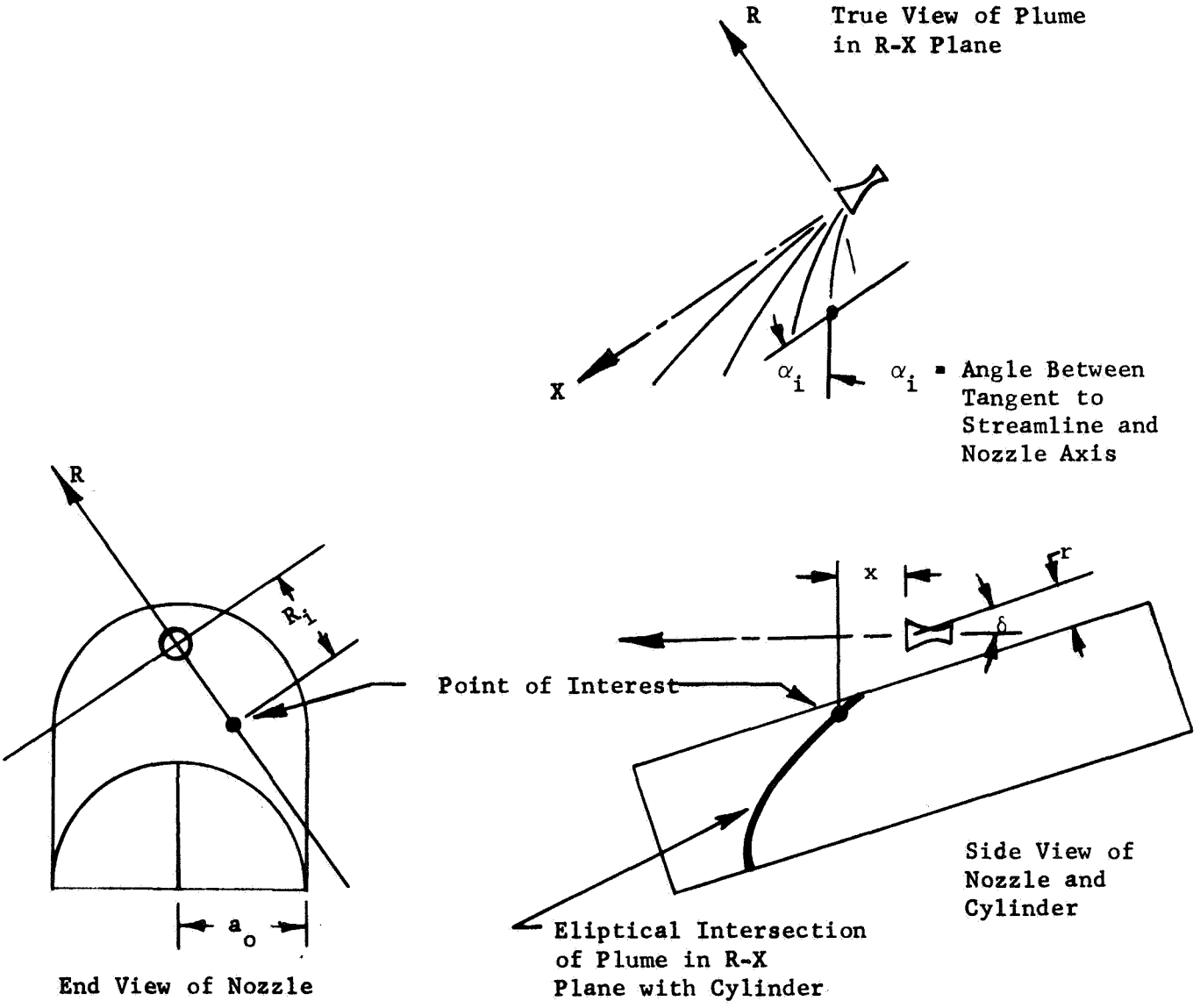

FIGURE 15b. **PITCH OR YAW ROCKET PLUME IMPINGEMENT ON A CYLINDRICAL SURFACE**

where:

$$\beta_i = \tan^{-1} \frac{R_i + (a_o + r) \sin \theta_i}{(a_o + r) \cos \theta_i}$$

$$\theta_i = \sin^{-1} \frac{R_i^2 + r\,(2a_o + r)}{2R_i\,(a_o + r)}$$

See Figure 15a for: R_i, P, a_o, α_i

Nozzle canted to surface ($\delta > 0$):

$$\text{True impingement angle} = \xi = \sin^{-1} \left[\cos \eta_i \sin \alpha_i \sin \beta_i - \sin \eta_i \cos \alpha_i\right]$$

where:

$$\eta_i = \tan^{-1} \left[\cos (\theta_i - \beta_i) \tan \delta\right]$$

$$\theta_i = \sin^{-1} \left[\sqrt{b_i^2 - C_i} - b_i\right]$$

$$b_i = \frac{R_o}{R_i \tan \delta} \qquad \phi_i = \sin^{-1} \left[\sin \theta_i \sin \phi\right]$$

$$C_i = \frac{a_o^2 - (R_o \cos \delta)^2 - R_i^2}{(R_i \sin \delta)^2}$$

$$\beta_i = \tan^{-1} \left[\frac{R_i \cos^2 \phi_i + R_o (\sin \phi_i \sin \delta - \sin \theta_i}{\cos \theta_i \left(R_i \sin \phi_i \sin \delta + R_o \cos^2 \delta\right)}\right]$$

See Figure 15b for R_i, R_o, δ, α_i, a_o

As can be seen from the above, the calculation of the true impingement angle can become a lengthy process. It is, however, possible to limit the number of off-center calculations by first obtaining the centerline distribution of pressure or heat transfer and then making impingement

profiles with only a few off-center calculations. Many cases will require calculation of only 4 or 5 specific points in one or two off-center plane intersections.

3.2 SURFACE PRESSURE

With the assumptions that the plume surface interaction shock and boundary layer are very thin, it is possible to estimate the pressure at the surface by simply turning the flow through the true impingement angle. The static pressure, Mach number, and specific heat ratio can be found at the point of impingement within the undisturbed plume. The true angle can be found as described in the previous paragraphs. The most accurate method for computing the static pressure in the flow after it has passed through the plume-surface interaction shock and turned parallel to the surface is somewhat debatable. There are three generally accepted methods available: (1) two-dimensional normal and oblique shock theory, (2) Newtonian impact theory, and (3) modified Newtonian impact theory. For a given case the resulting local surface pressure can vary as much as 30 percent depending on the method used. The most conservative solution is generally given by the two-dimensional, normal and oblique shock theory, while the lowest, and often unconservative, values of recovery pressure are given by the modified Newtonian method. Table 3 presents a comparison of the pressure rise calculated by the three methods for typical impingement conditions. The specific heat ratio was assumed constant at $\gamma = 1.25$. Note in this table that the pressure rise computed by the two-dimensional solution is surpassed by the Newtonian solutions only at very high angles of impingement.

TABLE 3

COMPARISON OF METHODS FOR COMPUTING THE PRESSURE RISE ACROSS NORMAL AND OBLIQUE SHOCKS

Impingement Angle	Flow Mach No.	Pressure Rise Ratio P_2/P_1		
		Two-Dimensional Shock Method	Newtonian	Modified Newtonian
23°	15	503	441	418
23	10	237	201	191
23	5	7.5	5.84	5.44
50	10	897	746	707
90	10	1110	1260	1205

A comparison of plume impingement pressure computed by the two-dimensional shock theory and the Newtonian theory is made with actual test results in Reference 14. The plume used for these calculations was constructed by a method of characteristics computer program using a constant specific heat ratio. It was found that the actual impingement pressure was more closely approximated by the two-dimensional theory in the region near the nozzle where the surface pressures are the highest. The Newtonian calculations provide a better fit to the data in very low pressure region several nozzle diameters downstream of the nozzle. It should be pointed out that the assumption of constant specific heat ratio (i.e., γ frozen at the nozzle exit plane) produces a plume with conservatively high local static pressure and temperature. If a variable γ plume were used (i.e., γ computed locally by the computer program as a function of local temperature), the two-dimensional shock theory will give a better approximation to the actual impingement pressure at distances farther from the nozzle. With the use of variable γ in the construction of the undisturbed plume, it is likely that the Newtonian solutions will result in low predictions of the local impingement pressure throughout the plume impingement region.

To minimize the potential of making low predictions of the local impingement pressures, only the two-dimensional shock theory is recommended and presented here.

Computer programs are generally available for computing oblique shock tables for various specific heat ratios at various increments of impinging angles and Mach numbers. However, the standard oblique and normal shock relationships may be solved by hand if necessary. The following equations for pressure and temperature rise across an oblique shock, Equations (6) and (7), can be solved using Equation (8). Equation (8) describes the relationship between the flow deflection angle, θ, which is assumed equal to the true impingement angle, and the shock wave angle, β. This equation may be solved by fixing θ and M, and iterating on β until both sides of the equation are equal. The value of β must be between $\sin^{-1}(1/M)$ and $\pi/2$.

$$\frac{P_2}{P_1} = 1 + \frac{2}{\gamma + 1}\left(M_1^2 \sin^2 \beta - 1\right) \tag{6}$$

$$\frac{T_2}{T_1} = 1 + \frac{2\,(\gamma - 1)}{(\gamma + 1)^2}\,\frac{M_1^2 \sin \beta - 1}{M_1^2 \sin^2 \beta}\left(\gamma M_1^2 \sin^2 \beta + 1\right) \tag{7}$$

$$\tan \theta = 2 \cot \beta \,\frac{M_1^2 \sin^2 \beta - 1}{M_1^2\,(\gamma + \cos^2 \beta) + 2} \tag{8}$$

Local velocity downstream of the oblique shock may be computed from Equations (7), (9), (10);

$$M_2 = \left\{ \frac{1 + \left(\frac{\gamma - 1}{2}\right) M_1^2 \sin^2 \beta}{\left[\sin^2(\beta - \theta)\right]\left[\gamma M_1^2 \sin^2 \beta - \frac{\gamma - 1}{2}\right]} \right\}^{1/2} \tag{9}$$

$$V_2 = M_2 \sqrt{\gamma g R T_2} \tag{10}$$

The use of the above Equations (6) through (10) requires the assumption that the gas is thermally and calorically perfect.

Figure 16 illustrates the relationship between θ, M_1, and β. It should be noted that for a given M_1 there is a maximum deflection angle (θ). This simply means that, if the flow must be deflected more than this maximum angle, an oblique shock is not sufficient and additional turning takes place in the shock layer flow. The pressure in this region is generally determined by normal shock relations. When the deflection angle is sufficiently large that the normal shock relations are to be applied, the local pressure and temperature rise across the normal shock may be computed using the following equations.

$$\frac{P_2}{P_1} = 1 + \frac{2\gamma}{\gamma + 1}\left(M_1^2 - 1\right) \tag{11}$$

$$\frac{T_2}{T_1} = 1 + \frac{2(\gamma - 1)}{(\gamma + 1)^2} \frac{\gamma M_1^2 + 1}{M_1^2}\left(M_1^2 - 1\right) \tag{12}$$

The use of these equations, of course, requires the assumption that the gas is thermally and calorically perfect.

With the information presented in the above paragraphs, it is possible to estimate the local plume impingement pressure profiles on flat or cylindrical surfaces. The local static pressure on the impingement surface is computed using the following steps: (1) establish the undisturbed exhaust plume profile, (2) determine the local static plume properties (P_1, M_1, γ) at the radial and axial location (located with respect to the nozzle) of the point of interest on the surface, (3) compute the true impingement angle, and (4) compute the local static pressure on the surface at the point of interest with the normal or oblique shock relations. Pressure profiles on the surface can be estimated by computing the static pressure on the line directly beneath the nozzle, and at several individual locations off this line, and combining the results graphically. Since the plume profile

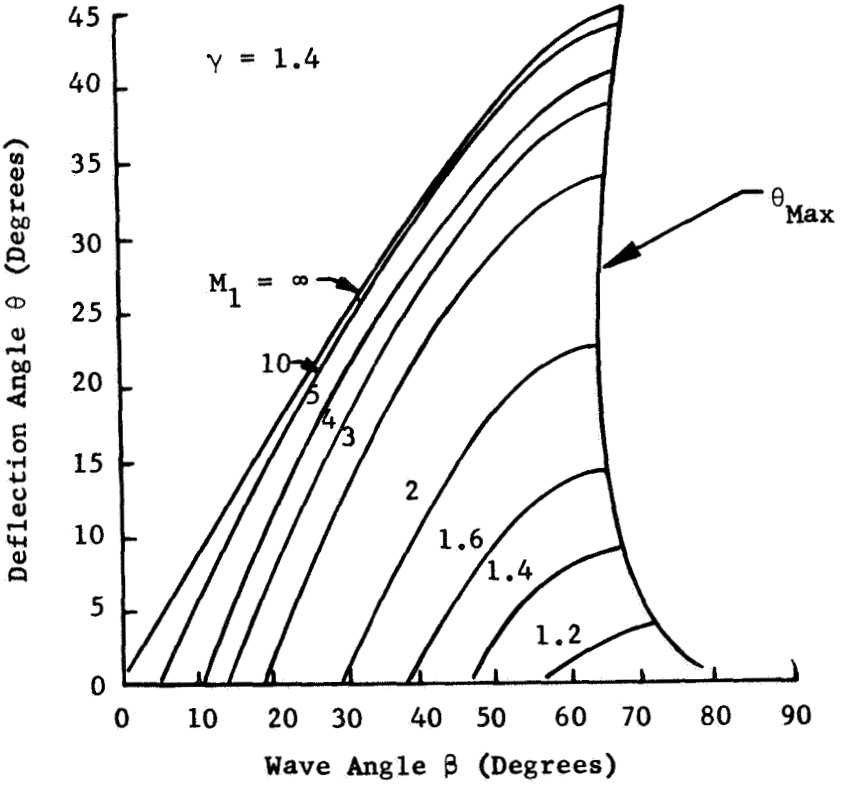

FIGURE 16 - OBLIQUE SHOCK SOLUTIONS

and the normal and oblique shock tables can be obtained with the use of computer programs, the most difficult part of the calculation becomes the solution of the true impingement angle. However, this presents a problem only for points on the surface which are not in a plane which is perpendicular to the surface and which contains the nozzle axis (i.e., the off-centerline points of interest).

Pressure profiles computed in the above manner may be used to estimate structural loading and true thrust vector of this motor. In addition, the pressure computed and the method used may be applied directly to estimating the heat transfer from the exhaust plume to the surface.

3.3 SURFACE HEATING

The primary objective of the above few paragraphs was to present a method for establishing the pressure profiles resulting from gas plume impingement on a surface. However, the methods for predicting the local temperature and velocity of the gas at the impingement surface was also presented above. This information can be used in estimating the surface heat transfer from the exhaust plume impingement.

Probably the best experimental data available on heat transfer from a real rocket plume impingement on a surface in a near space environment was obtained by North American Aviation for the Apollo program (see Reference 13). During these tests, a liquid rocket motor (about 90-pound thrust with Aerozine 50 and N_2O_4 as the propellant) was fired over a flat plate instrumented for pressure and heat transfer. Variables in these tests included nozzle area ratio, distance from the nozzle to the surface, and nozzle cant angle. Correlation of the heat transfer data was accomplished in Reference 14 by adding correlation constants to generally accepted methods for computing stagnation point and laminar flow flat plate convective heat transfer. It was found, in Reference 14 that over the entire range of test variables, the flow along the surface at the plate was laminar and in the continuum flow regime. The motor chamber pressure for these tests was nominally 100 psia. Since the range of test parameter (i.e., distance from the surface, nozzle area ratio, and motor cant angle) envelop most of the practical range for spacecraft application, and since solid rocket motors used in upper stage or spacecraft application will probably have more than 100 psia chamber pressure, it is reasonable to expect that the assumption of continuum flow will be valid. The assumption of laminar flow along the surface is probably also good since the density of the flow is low, and there is a favorable pressure gradient in the vacuum application.

The calculation of the heat transfer profile over a large surface requires the use of two separate heat transfer relationships: (1) stagnation heating (used in the normal shock region), and (2) laminar flat plate heat transfer (used in the oblique shock region). The general form of the Kemp and

Riddell empirical satellite re-entry heating equation (Reference 14) was used with an empirically determined constant to correlate the convective heat transfer in the normal shock region. Equation 13 is a simplification of the correlating equation presented in Reference 14.

$$q_N = \frac{55000\left(\frac{P_2}{RT_2}\right)^{1/2}}{\epsilon + \frac{3h}{4R_e}} \left(1 - \frac{T_2}{T_T}\right)^{1.625} \left(1 - \frac{T_W}{T_T}\right) \qquad (13)$$

where:

q_N = convective heat transfer in the normal shock region Btu/ft^2 sec)

P_2 = local static pressure at the surface (lb_f/ft^2)

R = gas constant (1544/molecular weight) ($ft\text{-}lb_f/lb_m\,^\circ R$)

T_2 = local static temperature at the surface ($^\circ R$)

ϵ = nozzle area ratio

h = distance of nozzle above the surface (inches)

R_e = nozzle radius (inches)

T_T = plume gas stagnation temperature ($^\circ R$)

T_W = surface temperature ($^\circ R$)

The above equation is applicable only in the normal shock region. It should be pointed out that the point of peak gaseous plume impingement heating has been found experimentally to coincide with the point of peak impingement pressure. Consequently, the location of the peak heating does not necessarily occur in the normal shock region. In fact, the peak impingement pressure, and heating generally occur in the oblique shock region.

The form of the Van Driest laminar flow equation (Reference 16) was modified with a correlating constant to approximate the heat transfer in the oblique shock region. A simplification of the equation, originally disclosed in Reference 14, is presented below (Equation 14).

$$q_o = 5.39\times10^{-9}(T_2)^{1.075}\ (M_2)^{2.39}\ (\gamma g)^{1.195}\ (R)^{0.695}\left(\frac{P_2}{Z}\right)^{0.5} \left[1 + \frac{5.88}{(M_2)^2}\left(1 - \frac{T_W}{T_2}\right)\right] \quad (14)$$

where:

T_2 = local static pressure at the surface (°R)

T_W = surface temperature (°R)

M_2 = local static Mach number downstream of the oblique shock

γ = plume specific heat ratio

g = 32.2 ($ft\text{-}lb_m/lb_f\ sec^2$

R = gas constant (1544/gas molecular weight ($ft\ lb_f/lb_m\ °R$)

P_2 = local static pressure at the surface (lbf/ft^2)

Z = distance measured from end of the normal shock region to the point of interest (ft)

It should be noted that the above equation will give erroneous solutions if the distance from the normal shock region (Z) becomes small. As previously mentioned, the peak surface heating coincides with the peak surface pressure. If the point at which the peak pressure occurs is in the oblique shock region, then Equation (14) is valid for locations downstream of that point. If, however, the point of peak pressure occurs in or near the normal shock region, then the maximum heating computed in the normal shock region should be used at (or extrapolated to) the point of peak pressure. Figure 17 illustrates the combination of the cold wall convective heat transfer rates from both the normal and oblique shock region for a typical centerline impingement heating case.

Surface heating profiles may be constructed in a manner similar to that described earlier for surface pressure profiles. The only significant problem in obtaining off-center heat transfer rates is establishing the proper length to be used in Equation (14) for the oblique shock region heat transfer. An approximation can be made by constructing on the surface pressure profile the line separating the normal and oblique shock regions, and drawing a line along the surface from the point of interest radially

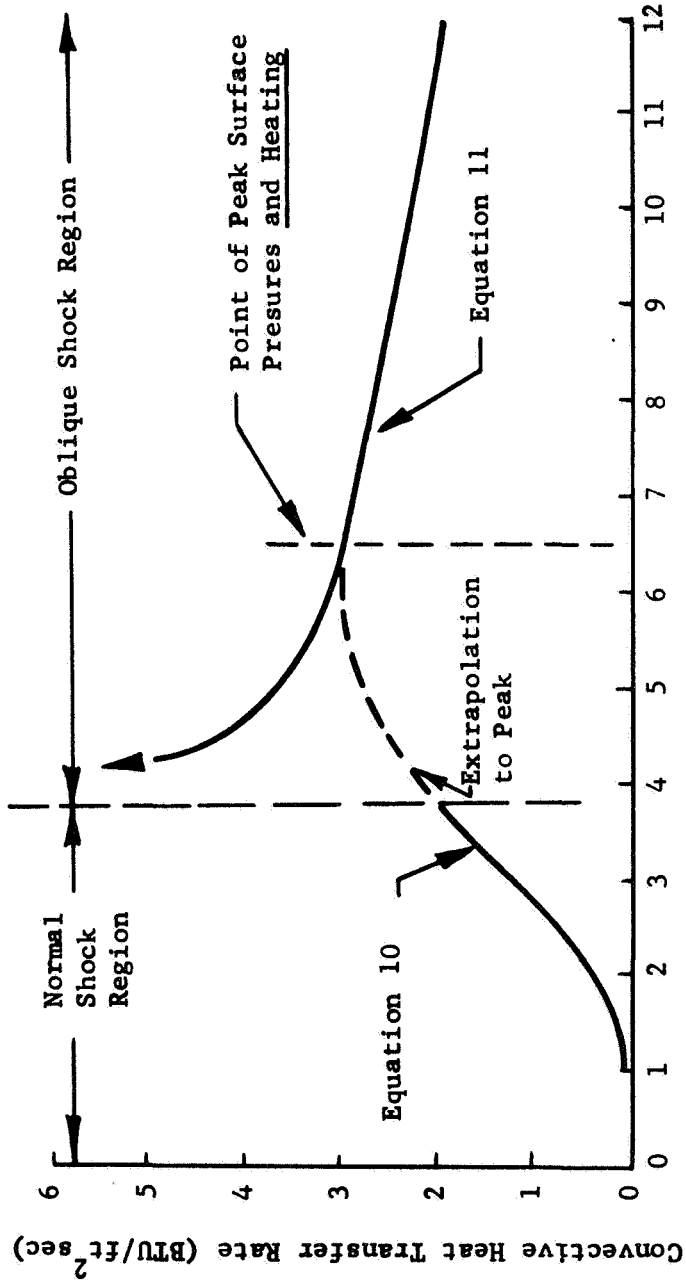

FIGURE 17. TYPICAL CONVECTIVE HEAT TRANSFER DISTRIBUTION

toward the nozzle. The distance along this line, from the point of interest to the line separating the normal and oblique shock regions, may be used to approximate the value of Z. Actual surface streamlines may be constructed from the true impingement angles; however, the additional calculations and plotting required are not commensurate with the additional accuracy gained.

With the information presented in the above paragraphs, it is possible to estimate the local plume impingement convective heating profiles on flat or cylindrical surfaces. The calculation of the convective heat transfer requires five general steps: (1) establish the undisturbed plume profile, (2) determine the local static plume properties (P_V,T_1,M_1,γ) at the radial and axial locations (located with respect to the nozzle) at the point of interest on the surface, (3) compute the true impingement angle, (4) compute the local static properties (P_2,T_2,M_2) on the surface at the point of interest with the normal or oblique shock relations, and (5) compute the local convective heating with the appropriate (normal shock or oblique shock region) convective heat transfer equation.

SECTION 4

CONCLUSIONS AND RECOMMENDATIONS

Using a helium flow facility to simulate the solid particle fluxes found in a solid rocket exhaust, it was found that aluminum experienced considerably less damage under particle cloud impaction than it would be expected on the basis of a collection of single particle impactions. These tests were run over a range of particle flux from 1 $gm/cm^2/sec$ to 8 $gm/cm^2/sec$. In addition, over this range of mass flux studied, high strength aluminum alloys were insignificantly better than essentially pure aluminum in resisting particle cloud erosion.

During the course of the helium flow tests, particle kinetic energy accommodation was measured. The kinetic energy accommodation factor was not observed to be higher than 10 percent and averaged about 8.5 percent for the materials tested and the range of mass flux studied.

A comparison of these results from this work with data from other sources made available during the course of the contract led to the discovery of the shielding effect caused by a buildup in front of the impinged surface of spent projectile material and surface ejecta. Because of the inelastic nature of the particle surface collision, reflected particles leave the surface with very low velocity and tend to accumulate in front of the surface with only gas drag as a means of removal. At sufficiently low particle mass flux, the incident particles reach the surface without interference. As the particle mass flux increases, the number of reflected particles increases so that collisions between incident and reflected particles become more frequent. As a result, some of the reflected particles are scattered back toward the target and strike a second time. Eventually, at sufficiently high particle mass flux, none of the incident particles strike the target surface without having experienced at least

one collision in the particle layer. As a result of the interparticle collisions within this debris layer, the incident particle momentum diffuses through the debris layer; a large fraction of this momentum is transferred to the target surface while most of the incident particle kinetic energy is absorbed by the layer, with only a small fraction (approximately 10 percent) transferred to the surface. This latter factor explains, at least in part, the reduced target damage experienced under particle cloud impaction.

Small scale solid propellant rocket firings in a vacuum chamber were used to produce particle mass fluxes ranging from 3×10^{-2} gms/cm^2/sec to 9×10^{-4} gms/cm^2/sec. A number of spacecraft materials, including coated aluminum, were placed in the exhaust flow of this rocket for periods ranging from 4-1/2 to approximately 6 seconds. In every case, the coatings were destroyed by a combination of the thermal and erosive effects of the flow. In one test in which the flow consisted of only hot exhaust gases, the gas heating effects alone were sufficient to destroy the coatings. The heat flux measured in this test was equivalent to a particle kinetic energy flux that would be obtained from a motor of the type used in these tests with a 12 percent aluminum propellant at a distance of about 400 inches from the exit plane.

A comparison of teflon impaction samples used in the rocket firings with other teflon samples used in the helium flow facility indicate that particle shielding was a significant factor over the entire range of particle incident mass flux used in these tests, which varied over 4 orders of magnitude from a flux of approximately 8 gms/cm^2/sec to 9×10^{-4} gms/cm^2/sec. The relative damage per impaction particle increased by a factor of 200 as the flux decreased between these two limits. It is likely that a similar increase in relative damage would be experienced with aluminum targets at much lower fluxes than were used in the laboratory tests in this program.

It is clear that there is a point far enough removed from the exit plane of a solid rocket such that the impacts on any surface are sufficiently infrequent that the damage from these impacts can be considered as a collection of single particle impacts. Between this point and that point where a shielding effect would begin to alter the incident particle stream at the surface, there is a region where particle impaction heating will be a significant factor and that a prediction of particle impaction damage would necessarily include a simultaneous continuous consideration of surface temperature. The significance of this factor depends on the thermal diffusivity of the surface and its effective strength. A particle shielding effect of the type discussed in this report has been seen to exist at particle fluxes of as low as 9×10^{-4} gms/cm^2/sec in a solid rocket flow impinging on a 1-inch-diameter specimen. It can be expected that this effect will be noted at much lower fluxes for larger bodies in practical situations.

A handbook type procedure was presented to aid in the evaluation of the effects of gaseous rocket exhaust plume impingement. This procedure can be used for making engineering estimates of the pressure and heat transfer distribution on a surface located within an exhaust plume. Of necessity, it was limited to highly underexpanded plumes and regions in which there were no plume shocks. The effect of the presence of a particle shielding layer, and/or gas-particle coupling, was not considered.

In order to be able to properly predict the impaction damage and kinetic energy accommodation on a spacecraft in a practical situation, it will be necessary to examine in greater detail the following areas: (1) the origin of aluminum oxide particles in the rocket motor should be studied more fully so that size and particle velocity distributions through the nozzle can be determined with the result that one could predict the particle mass and kinetic energy flux emanating from the rocket exit cone, (2) the physical properties of spacecraft materials such as aluminum, Teflon, and other polymetric materials, such as paints, should be measured over a range of temperature that is consistent with the temperatures that would be experienced in a typical spacecraft situation, (3) the nature of the particle shielding layer needs to be better understood over a range of particle incident mass flux that is typical of spacecraft situations of interest and a determination should be made of the important parameters that influence this phenomenon, and (4) the nature of the particle-surface interaction should be more fully studied; in particular, at velocities which would be typical of those experienced during the presence of a particle shielding layer. The existence of a particle size scaling effect should be determined for the materials that would be of interest, in spacecraft construction. The size and velocity of surface ejecta needs to be determined in order that the flow properties of the shielding layer could be determined.

REFERENCES

1. Sorensen, N. R., Proc. of Seventh Symposium on Hypervelocity Impact, Vol. VI, page 281 (1965).

2. Kuby, W. C., "Proposal for Effects of Impingement of Rocket Exhaust Gases and Solid Particles on a Spacecraft," Aeronutronic Proposal No. P-15244(U), submitted to JPL, August 1965.

3. Lewis, C. H., Hackett, R. D., and Kuby, W. C., Interim Report, "Effects of Impingement of Rocket Exhaust Gases and Solid Particles on a Spacecraft," Aeronutronic Division, Philco-Ford Corporation, JPL Contract No. 951246, 22 November 1966.

4. Dobbins, R. A., et al., "Measurement of Mean Particle Sizes of Sprays from Diffractively Scattered Light," AIAA Journal, Vol. 1, No. 8, Page 1882, August 1963.

5. Laderman, A. J., et al., Final Technical Report, "Study of Thermal Radiation, Particle Impingement Heating, and Flow Field Analysis of Solid Propellant Rocket Exhausts," Aeronutronic Division, Philco-Ford Corporation, Publication No. U-4045, Contract No. NAS8-20276, 19 April 1967.

6. Kuby, W. C., Fifth Monthly Progress Letter, "Effects of Impingement of Rocket Exhaust Gases and Solid Particles on a Spacecraft," Aeronutronic Division, Philco-Ford Corporation, JPL Contract No. 951246, 2 September 1966.

7. Fay, J. A., and Riddell, F. R., "Theory of Stagnation Point Heat Transfer in Dissociated Air," J. Aero. Sci., 25, 73-85, 1958.

8. Boison, J. C., Curtiss, H. A., "An Experimental Investigation of Blunt Body Stagnation Point Velocity Gradient," ARS Journal, Page 130, February 1959.

9. Lewis, C. H., and Carlson, D. J., "Normal Shock Location in Underexpanded Gas and Gas Particle Jets," AIAA J, 2, 776, 1964.

10. Laderman, A. J., Lewis, C. H., and Byron, S. R., "Two Phase Plume Impingement Forces," Final Report, Aeronutronic Division, Philco-Ford Corporation, Aeronutronic Publication No. U-4429, SAMSO TR-68-308, August 1968.

11. Denardo, B. P., and Nysmith, C. R., "Momentum Transfer and Cratering Phenomena Associated with the Impact of Aluminum Spheres into Thick Aluminum Targets at Velocities to 24,000 ft/sec," Paper presented at AGARD Fluid Dynamic Panel Specialists Meeting, Marseille, France, April 1964.

12. Moore, H. J., Gault, D. E., and Heitowit, E. D., "Change of Effective Target Strength with Increasing Size of Craters for Hypervelocity Impact Craters," Proceedings of Seventh Hypervelocity Impact Symposium, Vol VI, 1965, pp. 371-381.

13. Vick, A. R., and Andrews, E. H., Jr., "An Experimental Investigation of Highly Underexpanded Free Jets Impinging upon a Parallel Flat Plate," NASA Langley, unpublished as of September 1963.

14. Piesik, E. T., and Lofland, M. L., "High-Vacuum Plume Impingement Test Report," North American Aviation (S&ID) Accession No. 86086-64, August 1964.

15. Kemp, N. H., and Riddell, F. R., "Heat Transfer to Satellite Vehicles Re-entering the Atmosphere," Jet Propulsion, Vol 27 (February 1967).

16. Van Driest, E. R., Investigation of Laminar Boundary Layer in Compressible Fluids Using the Crocco Method, NACA TN 2597 (1952).